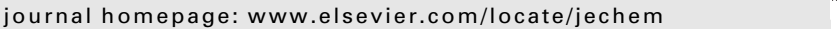


Contents lists available at ScienceDirect

Journal of Energy Chemistry





ttp://www.journals.elsevier.com/

Discrete composition control of two-dimensional morphologic all-inorganic metal halide perovskite nanocrystals

Andrew Hunter Davis, Weiwei Zheng*

Department of Chemistry, Syracuse University, Syracuse, NY 13244, United States

ARTICLE INFO

Article history: Received 7 August 2020 Revised 5 October 2020 Accepted 10 October 2020 Available online 1 November 2020

Keywords: All-inorganic perovskites Two-dimensional nanocrystals Composition Doping Alloying Ion exchange

ABSTRACT

Metal halide perovskite nanocrystals (NCs) exhibit impressive optical and electronic properties, making them an important class of functional materials with promising applications in solar cells, light emitting diodes (LEDs), photodetectors, and photocatalysts. In addition to the widely studied 0-dimensional (0D) metal halide perovskite NCs, such as nanocubes, low dimensional perovskites, such as 2D all-inorganic perovskite (AIP) NCs, subsist with directionally relevant quantum confinement. These anisotropic NCs have the propensity to exhibit interesting optoelectronic properties that are exceedingly difficult to introduce into 0D systems, yet as of late are largely unexplored. In this review, we discuss the recent synthetic progress of 2D all-inorganic metal halide perovskite NCs with ABX₃ structure. Specifically, we highlight the discrete composition control of the cations (A and B sites) and anions (X site) by dopant incorporation and alloying in 2D metal halide perovskite NCs. We will also discuss more complex perovskite crystal structures, such as Ruddlesden–Popper double perovskites, and compare these materials to 0D perovskite systems. Ultimately, our work culminates in the future interests and perspectives of this field with a focus on the wide applicability of 2D systems and the large variance in structure capable with discrete compositional tuning.

© 2020 Science Press and Dalian Institute of Chemical Physics, Chinese Academy of Sciences. Published by ELSEVIER B.V. and Science Press. All rights reserved.

1. Introduction

Metal halide perovskite nanocrystals (NCs), of general ABX₃ structure, are a newly emerging material with promising applications in optoelectronics devices, including solar cells [1-6], solar concentrators [7], light emitting diodes [5,6,8], visible light communication [6,9-11], lasers [4,6,12,13], photodetectors [11,14], non-linear optics [15], as well as in photocatalysis [16,17] and other charge transport applications [11,18,19]. The A-site of this structure consists of a monovalent organic or inorganic cation such as, methylammonium (MA, CH₃NH₃), formamidinium (FA, CH (NH₃)₃⁺), Cs⁺, or Rb⁺, while the B-site is occupied by a divalent cation such as Ge²⁺, Pb²⁺, or Sn²⁺, and the X-site is a halide anion such as Br⁻, Cl⁻, I⁻, or a mixture thereof [20-23]. Initially, organic-inorganic "hybrid" perovskite NCs, such as methylammonium lead bromide (MAPbBr3), were the main focus of development because of their low fabrication cost, large absorption cross sections, high photoluminescent quantum yields (PL QYs), low exciton binding energies, high in plane charge mobility, defect tolerance, and long electron and hole diffusion lengths [3,24-27].

However, these hybrid materials suffer from environmental and thermal instability leading to the prevalence of "all-inorganic" perovskite NCs [20,28–32].

All-inorganic perovskites (AIP), consisting of inorganic A and Bsite cations, are a more stable alternative to their hybrid organicinorganic counterparts, due to their increased thermal stability, while also exhibiting impressive optical and electronic properties [33–38]. The continued development of perovskite-based devices and applications relies on the availability of dependable synthetic methods with controlled composition, size, and morphology [4,21,39–41]. Due to the ionic nature of perovskites, the composition control of AIP NCs is more flexible than that of traditional metal chalcogenide semiconductor NCs. Synthetic manipulation can vary chemical composition in the cation and anion sites, with post-synthetic manipulation to provide further control through ion-exchange and exfoliation. The synthetic versatility of AIP NCs has, therefore, created some of the most widely tunable materials ever produced, with the resulting color tunability spanning from UV to near-IR emissions [42-47].

For metal halide perovskite NCs with ABX₃ structure, two main strategies are available for discrete compositional control, including alloying and doping in the A, B, and X-sites, resulting in more stable, highly luminescent, and even dilute magnetic NCs (Table 1)

^{*} Corresponding author. E-mail address: wzhen104@syr.edu (W. Zheng).

Table 1Compositional control of A and B-sites of 2D ABX₃ AIP NCs.

Site	Impurity ion	[Impurity ion]	Host AIP lattice
A-site	FA ⁺	33%	CsPbBr ₃ , CsPbBr _x I _{3-x} , and CsPbI ₃ NSs [65]
	Rb ⁺	40%	CsPbBr ₃ NPLs [66]
B-site	Mn ²⁺	0.2%-35%	CsPbCl ₃ NPLs [67–71]
		4.3%-15%	CsPbBr ₃ NPLs [72,73]
		1.7%	Cs ₂ PbCl ₂ I ₂ NPLs [74]
	Ni ²⁺	0.1%	CsPbBr ₃ NPLs [75]
	Sn ²⁺	3.4%	CsPbBr ₃ NPLs [76]
	Sb ³⁺	1.5%	CsPbI ₃ NPLs [77]
	Yb ³⁺	1.4%	CsPbBr ₃ NPLs [73]

[48-53]. Doping, dominantly in the B-site, entails the intentional introduction of small amounts of impurity ions (generally only a few percent in concentration) within the lattice of a host NC, leading to minor changes in composition that can be used to tune the NCs properties, such as improving structural stability, incorporating magnetic spin centers, and introducing new optical pathways in perovskite NCs [50,51,54-61]. Meanwhile, alloying, mainly in the A- and X-sites, involves depositing a relatively large quantity of ions into a host lattice to cause wide-scale structure changes. Table 1 summaries compositional control of A and B-sites of 2D ABX₃ AIP NCs, while X-site alloying is not summarized as it is mainly by halide exchange between Cl, Br, and I. As such, doping and alloying have been widely used for tuning optical, electronic, and magnetic properties; offering methods of improving existing properties while incorporating novel functionality [56,58,61-64]. There has yet to be a fine line drawn to distinguish the exact concentrations of impurities required for doping vs. alloying in perovskite NCs, thus we will be discussing doping and alloying in this report according to the location of ion incorporation in the interest of simplicity. Therefore, A and X-site ion incorporation will be deemed alloying due to an abundance of reports showing large incorporation concentrations, while B-site ion incorporation will be deemed doping as the majority of incorporation reports involve small concentrations.

Generally, A-site alloying is used to alter the NC composition without causing large alterations to the NC bandgap, thus utilized for NCs with favorable optical properties, such as to maintain the small bandgap and red-light PL of CsPbI₃ NCs. However, large scale incorporation can cause disparity in optical, electronic, and structural properties. For example, Cs⁺ incorporation has been widely used to improved thermal stability in hybrid organic-inorganic lead-based ABX₃ NCs, such as FAPbX₃ [78-80] and MAPbX₃ [81,82] NCs. On the other hand, X-site anion exchange and alloying is used for an opposing approach where the backbone of the perovskite structure is heavily altered, resulting in drastic changes to optoelectronic properties and structural stability. Therefore, Xsite anion exchange and alloying has been widely utilized in iodine containing compounds, such as CsPbI₃. This is because, the optically active cubic phase CsPbI₃ is far too unstable to be utilize normally, thus X-site ion exchange and alloying is often used to further stabilize these structures by Br incorporation, even though a slight to large blue shift occurs based on the concentration incorporated due to broadening of the NC bandgap [83–87].

Progress surrounding shape control has led to the development of all-inorganic metal halide perovskites ranging in structure from 0-dimensional (0D) nanocubes to 1D nanorods (NRs) and nanowires (NWs), to 2D nanoplatelets (NPLs) and nanosheets (NSs) [88–94]. Of these systems, 2D nanomaterials are of keen interest for their impressive optoelectronic properties [5,18,95,96], including extremely narrow absorption and emission spectra [67,88,90,97,98], high absorption cross sections [97,99], increased surface-to-volume ratios [97,100], polarized and chiral emissions

[99,100], improved dielectric properties [98,101], high color tunability [95,97,98,101,102], and ease of direct application particularly in layered devices [67,88,98,100,101], in comparison to more traditional 0D NCs. Therefore, the development of high-quality and reliable syntheses for 2D AIP NPLs and NSs with well-defined morphologies and composition are critical for future device applications.

While the manipulation of composition through doping and alloying of organic-inorganic "hybrid" halide perovskite NCs has been widely reported [49,103–115], the field of discrete composition control of 2D AIP NCs is still in its infancy, with only a handful of publications on doped or alloyed 2D AIP NCs reported to date [67–74,116–124]. However, compositional control in 2D AIP NCs has shown unique properties compared with those in 0D AIP NCs. For instance, Mn-doped CsPb₂Br_{5-x}Cl_x NPLs have shown up to a 10-times greater host-to-dopant energy transfer efficiency than the same nanocube system. This massive increase could be associated to increased doping concentration per particle due to NPLs large surface-to-volume ratio, yet, even when normalized for dopant concentration the resulting host-to-dopant energy transfer still increases by 2.8 fold with NPLs compared to nanocubes [117].

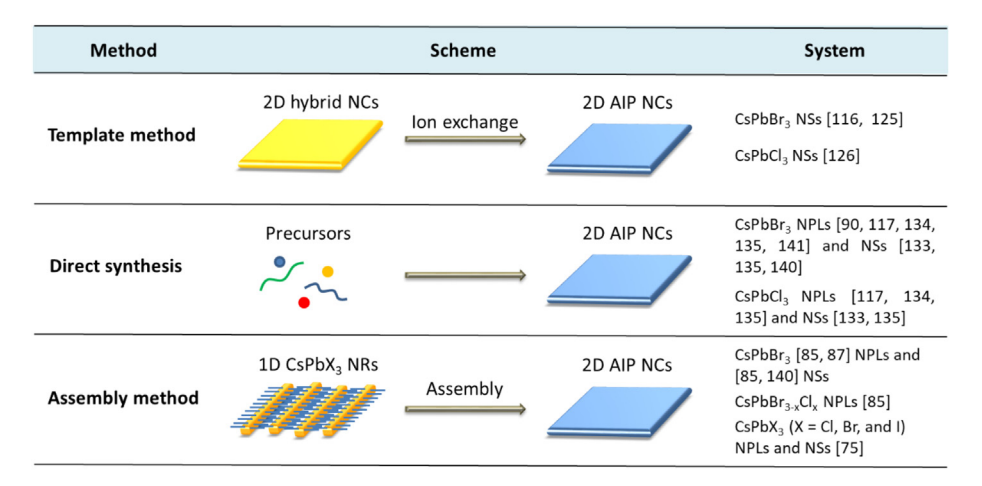
In this review, we wish to primarily shine light on the synthetic, compositional, and morphological control of 2D AIP NCs. While we will not be largely covering the composition control of colloidal organic-inorganic, 0D colloidal AIP NCs, or heterostructure materials, there are many great review articles that we would recommend for the reader interests [4,21,23,100,109,112,125–129]. Our intention is to illuminate the virtues of doping and alloying strategies of 2D AIP NCs to expose their importance for the further development of functional 2D perovskite NCs toward real world applications. To do this, we have broken down the key components of shape and composition control of 2D AIP ABX₃ perovskite NCs into four sections; 1) synthetic strategies for 2D AIP NCs; 2) A and X-site alloying and ion exchange; 3) B-site doping; and 4) applications of 2D AIP NC. The challenges and future directions of the field including stability issue of AIP NCs are also discussed.

2. Synthetic strategies for 2D All-Inorganic metal halide perovskite NCs

Generally, OD AIP NCs, such as nanocubes, are synthesized by the hot-inject of a Cs-oleate precursor into a solution of PbX₂ and organic solvents at elevated temperatures [21,130,131]. However, 2D AIP NC growth generally requires highly deliberate control of experimental parameters, including temperature [122,132], ligand diversity [88,102], ligand concentration [70], and ligand hydrocarbon chain length [88,102,132]. The formation of 2D nanomaterials is often difficult as the increased reactive surface area often leads to decreased thermal and chemical stability, nevertheless the development of 2D perovskite NCs is still well underway, providing several methods for the controlled synthesis of these materials. So far, there are three methods developed to synthesize 2D AIP NCs including: 1) template mediated synthesis of 2D AIP NCs, 2) direct synthesis of 2D AIP NCs by manipulating ligands, pressure, temperature, and composition, and 3) the assembly strategy for 2D AIP NC growth (Scheme 1). These methods are of keen interest to current and forthcoming works as each has led to the further development of doped and/or alloyed 2D nanomaterials that can improve AIP NC properties and stability for future applications.

2.1. Template mediated synthesis of 2D inorganic NCs

A traditional template method forces the formation of NCs in a specific shape based on the area/dimensionality provided and driv-



Scheme 1. Schematic detailing the three different synthetic procedures for 2D AIP NCs.

ing forces for the reaction. This way, the formation of otherwise complex shaped NCs can be more easily and readily obtained. Therefore, it is possible to use a previously synthesized organic-inorganic hybrid perovskite NC as a template for the controlled formation of 2D AIP NCs.

A recent study by Zeng et al. [121] utilized a 2D hybrid perovskite, octadecylamine (ODA*) lead bromide (ODA₃PbBr₃), as a template for 2D CsPbBr₃ through a facile cation exchange method, by the introduction of a cesium acetate salt as a Cs* precursor at room temperature. The cesium precursor was dispersed in a solution of acetic acid, which upon introduction into the toluene solution containing the previously synthesized 2D ODA₂PbBr₄NSs (Fig. 1a) forced Cs* to replace the ODA* cation, forming thicker high quality 2D CsPbBr₃ NCs (Fig. 1c). The exchange process of Cs* for ODA* in ODA₂PbBr₄ was found to be favorable due to a decrease in the Gibbs formation enthalpy upon product formation. Meanwhile, the NCs maintained their 2D morphology due to Cs⁺ forcing the assembly of the [PbBr₆] sublayers previously sandwiched by ODA⁺ bilayers [121]. Interestingly, NC thickness increased with increasing Cs⁺ dose, as more ODA₂PbBr₄ octahedral layers merged to form CsPbBr₃ NSs, causing a distinct red-shift in the PL spectra (Fig. 1b and d). A clear trend in NC thickness was observed based on the dose of Cs⁺ introduced into the 2D NC system, with larger quantities of Cs⁺ resulting in thicker homogeneous NSs and lower Cs⁺ quantities resulting in poor homogeneity due to partially substituted ODA⁺ ions remaining in the NCs; causing the presence of NSs of varying thicknesses [121].

The template method provides great synthetic control by varying B and X-sites of the 2D templates prior to the A-site Cs⁺ cation exchange. This is especially true when comparing 2D hybrid to AIP

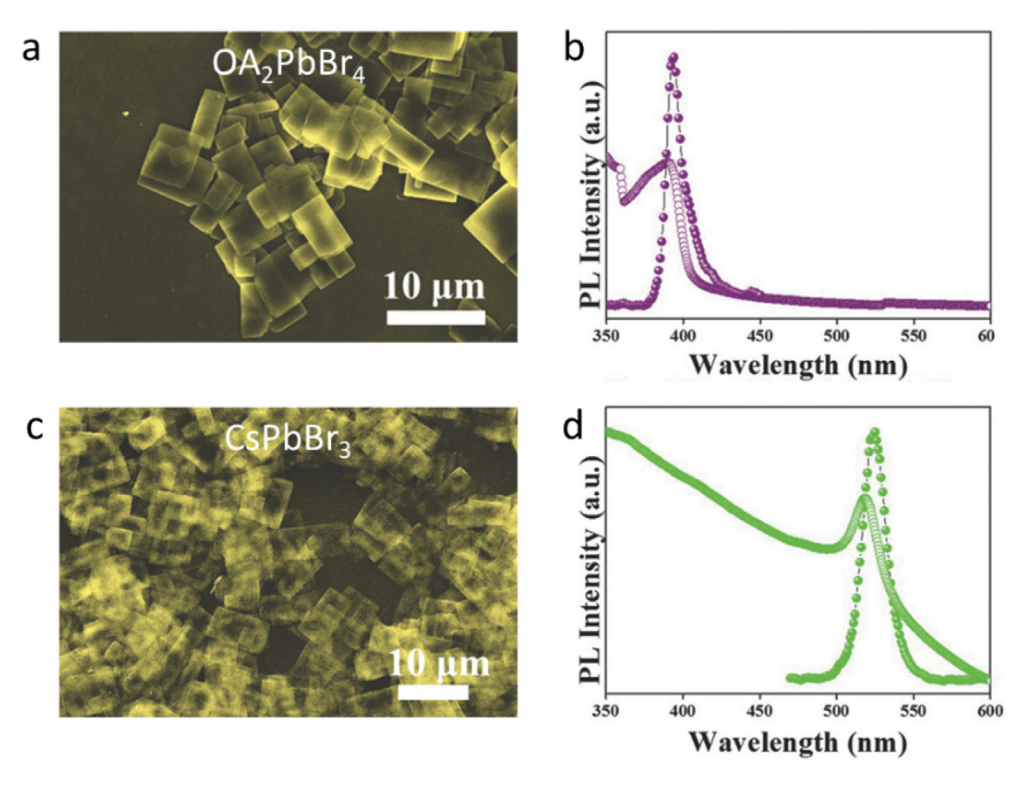


Fig. 1. SEM images of (a) OA₃PbBr₃ NSs and (c) CsPbBr₃ NSs. Absorbance and PL spectra of (b) OA₃PbBr₃ NSs and (d) CsPbBr₃ NSs. Adapted from Ref. [121] with permission from the John Wiley & Sons, Inc publishing group.

NCs as hybrid 2D structures have been more heavily studied due to their impressive optoelectronic properties and improved moisture stabilities. Synthetic enhancement of the template mediated method was further propagated by Yu et al., who showed that post-synthetic ultrasonication treatment of the as synthesized ODA₂PbBr₄ NSs resulted in a more crystalline and monodisperse precursor to produce higher quality CsPbBr₃ NSs. As a result, the ODA₂PbBr₄ NS with higher crystallinity and narrower FWHM were obtained, which in turn resulted in higher crystallinity and increased PL QY in the synthesized CsPbBr₃ NSs, following a similar cation exchange method [133]. More recently, CsPbCl₃ NSs were synthesized by a similar post-synthetic cation exchange method that utilized ODA₂PbCl₄ NSs as the intermediate precursor [134].

2.2. Direct synthetic manipulation by control of reactive environments

The template method discussed in 2.1 can be applied to synthesize 2D AIP NCs, however, with the drawback that more time, effort, and materials must be utilized in order to first develop the template that will guide the desired NC formation. Therefore, direct synthesis and growth of 2D AIP NCs is highly desirable. Early studies indicate that composition, temperature, and ligand environment are highly effective to control morphological formation of perovskite NCs. To this end, perovskites have shown the keen ability to be drastically varied in shape by manipulation of ligand, pressure, temperature, and composition, making 2D AIP NCs highly prominent for structural and shape manipulation [70,88,135–140].

In one such case, Xie et al. reported a facile heat-up approach for AIP CsPbX₃ (X = Cl, Br, I, and mixtures thereof) NCs by directly heating all the precursors with solvent/ligands in open air. The resulting AIP NCs could be highly varied from 0D QDs to 2D NPLs and NSs by adjusting the reaction temperature, time, ligand species, and halide precursors. (Fig. 2) [122]. As such, they showed that 2D CsPbCl₃ NPLs (Fig. 2b and d) can be produced at 95 °C with oleylamine (OAm) and oleic acid (OA) as the capping ligands, and 2D CsPbBr₃ NPLs can also be synthesized at slighted higher temperatures from 100 to 160 °C (Fig. 2f and h), yet 0D (Fig. 2a and d) and 1D CsPbl₃ NCs were formed at 95–110 °C. Further manipulation of these NCs could be realized by manipulating the reaction

time, temperature, and ligand environment of the system. The best example of this is the CsPbBr₃ system, where they showed that by replacing OAm with octylamine (OctAm) caused the formation of larger NSs (Fig. 2g and h) rather than NPLs. Additionally, variance of the reaction temperature afforded nanocubes between 90 and 100 °C (Fig. 2e and h), while the NPLs and NSs formed at 110 °C [122].

Yang et al. [141] observed the evolution of 0D CsPbX₃ (X = Br, Cl, I) nanocubes to a mixture of 1D nanorods (NRs) and 2D square-shaped NSs with increasing reaction time using a hot-injection method with reaction temperatures ranging from 150 °C for CsPbBr₃ and CsPbCl₃ NCs to 250 °C for CsPbI₃ NCs. Briefly, reaction times of less than 10 min for CsPbBr₃ and CsPbCl₃ produced nanocubes, while longer reaction times, resulted in the formation of large NWs, with NSs also present in solution. CsPbI₃ 1D NRs and 2D NSs can also be synthesized by a similar method requiring higher temperatures. No evidence was found to suggest that the NWs and NSs formed by oriented attachment driven by dipole interactions, rather, the NW growth was attributed to surfactant mediated growth as the NWs were found to be more prevalent in systems containing higher concentrations of OAm [141].

Zhang et al. furthered the direct synthetic approach via a swift and versatile microwave assisted reaction method to synthesize 0D QDs, 1D NRs, and 2D NPLs [142], in which cesium acetate and $PbX_3(X = Cl, Br, I, and mixture thereof)$ were added to a mixture of OA, OAm, trioctylphosphine oxide (TOPO), and ODE in a microwave tube and heated for 5 min at 80 to 160 °C. The morphology was tuned by temperature and precursor dissolution, in which 160 °C produced QDs, 80 °C produced NPLs, and NRs were formed by first dissolving the precursors in a flask at 60 °C and then treating the crude sample in the microwave tube at a range of temperature from 80 to 160 °C [142].

Ligand mediated synthetic control was also displayed by Manna et al. [143], where 2D CsPbBr $_3$ NPLs and NSs could be synthesized by the introduction of a mixture of shorter capping ligands (octanoic acid (OctA) and OctAm) and long capping ligands (OA and OAm). By tuning the ratio between the short and long capping ligands in solution, NPLs and NSs of differing lateral dimension form 300 nm to 5 μ m could be synthesized without varying the

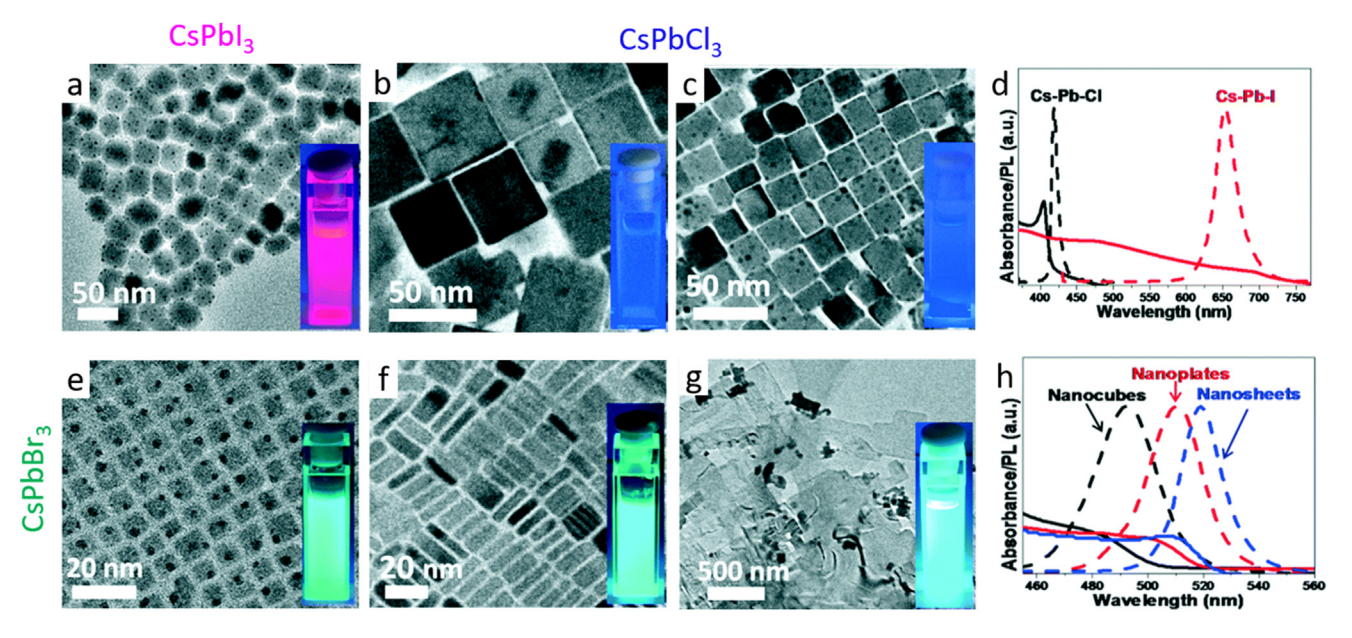


Fig. 2. TEM images of (a) CsPbI₃ nanocubes, CsPbCl₃ NPLs with (b) OAm and (c) OctAm ligands, as well as CsPbBr₃ (e) nanocubes, (f) nanoplatelets, and (g) nanosheets. Absorbance and photoluminescent spectra for the as synthesized (d) CsPbCl₃ NPLs (black) and CsPbI₃ nanocubes (red) and (h) CsPbBr₃ nanocubes (black), nanoplatelets (red), and nanosheets (blue) with respect to wavelength. Adapted and modified from Ref [122] with permission from the Royal Society of Chemistry.

2D NC thickness. The optimized reaction conditions were at 155 °C and under 5 min reaction time for the highest quality 2D CsPbBr₃ NCs. Given these experimental parameters, small concentrations of short ligands result in smaller NPLs and higher concentrations promoting growth of larger NSs up to 5 μ m in size [143].

Morphology of 2D AIP NCs has been further controlled through the variance of 2D NC thickness, resulting in large changes in quantum confinement and therefore optical and electronic properties. For example, Manna et al. [102] developed a hot-injection method under open air conditions to synthesize thickness controlled CsPbBr₃ NPLs by quickly injecting a PbBr₂ precursor, dissolved in N,N-dimethylformamide, into a mixture of Cs-oleate, 1octadecene (ODE), OAm, OA, and HBr, which was then guenched by the addition of acetone. The thickness was controlled by the amount of concentrated HBr introduced in solution, with increasing quantities resulting in thinner NPLs (Fig. 3a-c). Samples without HBr formed ~3.0 nm thick (5 monolayer (ML)) and ~8 nm by ~41 nm lateral NPLs, while those containing the maximum 7.5 µL HBr produced 1.8 nm thick (3 ML) NPLs (Fig. 3d and e). 2D CsPbI₃ and CsPbCl₃ NPLs were further synthesized using an anion exchange method (Fig. 3f). The thickness control stems from an abundance of H⁺ in solution, which protonates OAm, effectively

slowing the NCs growth by competing with Cs⁺ for surface binding sites [102,144,145]. Therefore, the more acidic the solution, the more protonated OAm ligands that can strongly bind to thin NPL surfaces to stop them from growing along the vertical direction. Similarly, Xie et al. [119,146], showed that incorporating Sn⁴⁺ or trivalent ions (In³⁺, Bi³⁺, and Al³⁺) onto the surface of CsPbX₃ NPL resulting in competition between the surface adhered ions and Cs⁺ and therefore produced thinner NPLs.

2.3. The assembly strategy for 2D AIP NC growth

Further exploration of ligand-controlled syntheses for 2D perovskite NCs has been made in the form of post-synthetic manipulation. Alivisatos et al. [99] reported the lateral oriented attachment of CsPbBr₃ NPLs to form CsPbBr₃ NSs. Their work showed that modifying a previously reported CsPbBr₃ nanocube hot-injection method, established by Protesescu et al. [147], by lowering the reaction temperatures from 140–200 °C to 90– 130 °C would preferably produce 2D NPLs instead of NCs with the original nanocube morphology. In this case it was found that the temperature correlates to the resulting thickness of the particles, with temperatures around 130 °C producing 3 nm thick

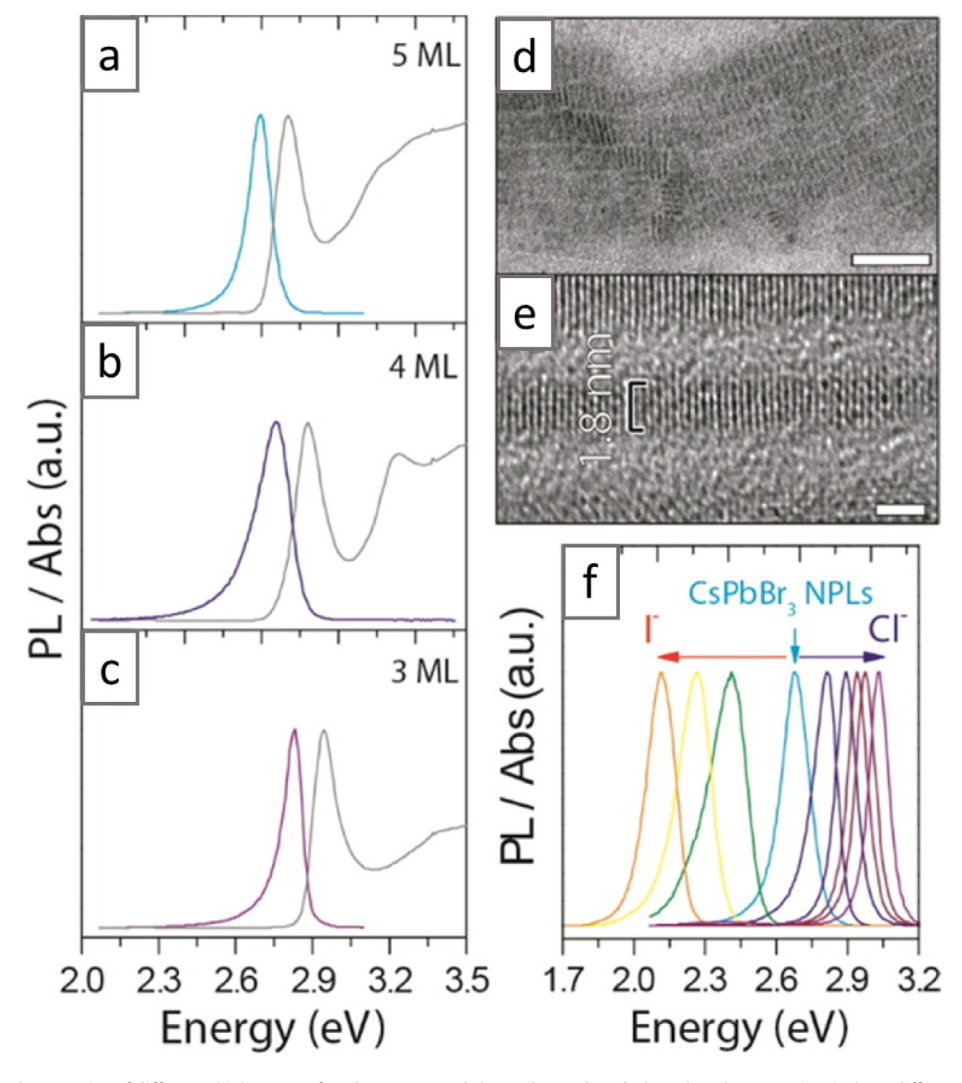


Fig. 3. Optical and structural properties of different thicknesses of CsPbBr₃ NPLs and the exchanged CsPbCl₃ and CsPbl₃ NPLs. (a-c) Three different thicknesses, with (a) 5 ML emitting at 2.70 eV and fwhm = 0.11 eV; (b) 4 ML emitting at 2.76 eV and fwhm = 0.17 eV; and (c) 3 ML emitting at 2.83 eV and fwhm = 0.09 eV. (d and e) TEM and HRTEM image of 3 ML thick sample indicated a thickness of 1.8 nm. (f) Finetuning the PL of CsPbBr₃ NPLs with anion-exchange reactions to CsPbCl₃ and CsPbl₃. Scale bar corresponds to 50 nm in (d), and 2 nm in (e). (Reproduced with permission from the ACS, https://pubs.acs.org/doi/10.1021/jacs.5b12124, Ref. [102]. Further permissions related to this material excerpt should be directed to the ACS.)

20 nm lateral NPLs while larger NPLs with 200–300 nm in lateral dimensions could be formed with thicknesses down to a single unit cell at around 90–100 °C. Further NPL assembly occurred by two methods, face to face column stacking and lateral crystallographically oriented attachment. The former resulted from strong ligand-ligand interactions at the surface of the NPLs in highly concentrated solutions while, the latter resulted from ligand destabilization in dilute solutions [99].

It is worth noting that, despite the success in formation of 2D CsPbBr₃ NCs via many approaches; 2D CsPbCl₃ and CsPbI₃NCs are generally obtained by anion exchange in the presence of Cl- and I⁻ anions [99,148]. To overcome this limitation, our group previously developed a two-step process to grow 2D CsPb X_3 (X = Cl, Br, I) NPLs and NSs by the ligand-mediated assembly of corresponding 1D NRs under solvothermal conditions (Fig. 4) [88]. In the first step, 1D CsPbX₃ (X = Cl, Br, I) NRs were synthetized using a hot-injection method by reacting Cs-oleate with PbX_2 (X = Cl. Br. I) in a mixture of long-chain capping ligands (OA and OAm), shorter ligands (OctA and OctAm) and ODE at 80-120 °C. The selective adhesion of ligands on different facets of NCs led to anisotropic growth of 1D NRs. Subsequently, 2D CsPbX₃ NPLs and NSs were formed by the assembly of the corresponding NRs in a Teflonlined stainless-steel autoclave under solvothermal conditions at 160 °C for 1–5 h (Fig. 4). It is believed that the relatively high pressure under solvothermal conditions can facilitate spatial constraint by decreasing the viscosity of the growth medium and the free volume available for 1D NRs dispersion [149-151], which induces 1D to 2D shape transition from the assembly of the NRs, eliminating high-energy surfaces and therefore reducing the total surface energy of the NCs. Interestingly, the lateral size of the 2D NCs is proportional to the solvothermal growth times with three well-defined stages for CsPbCl₃ and CsPbBr₃ (Fig. 4a–i). The increased solvothermal treatment time of the small 2D NPLs (stage I) led to further assembly of small NPLs by z-direction stacking and lateral fusing, in which larger irregular NPLs, accompanied by small NPLs, were obtained in stage II and much larger NSs were obtained with further extended solvothermal treatment time in stage III [88].

The 2D CsPbI₃ NPLs can also be obtained using the assembly of 1D CsPbI₃ NRs under solvothermal conditions (Fig. 4n). However, the growth of 2D CsPbI₃ NPLs requires less solvothermal treatment time (<1.5 h) compared with those for CsPbCl₃ and CsPbBr₃ NPLs due to the fast reaction kinetics. With the increasing of solvothermal treatment time, big 1D CsPbI₃NRs were obtained (Fig. 4l and 4 m) due to rapid cubic to orthorhombic phase transition since orthorhombic CsPbI₂ does not have a 3D corner-sharing [PbI₆] network, but instead contains ribbons of edge-connected [PbI₆] octahedra with only quasi-2D connectivity [152], leading to 1D NC growth. Interestingly, the growth of cubic phase CsPbBr_{1.5}I_{1.5} alloy NPLs and NSs can be achieved by the assembly of CsPbBr_{1.5}I_{1.5} NRs without phase transition. The cubic phases of the perovskite CsPbBr_{1.5}I_{1.5} alloy NPLs are fluorescent active and have great potential in practical photovoltaic applications. This work describes the first general strategy for the growth of 2D all AIP NCs including 2D CsPbCl₃, CsPbBr₃, CsPbI₃, and CsPbBr_{1.5}I_{1.5} NCs without the assistance of anion exchange, to the best of our knowledge.

A similar report by Zhong et al. presents a pre-dissolution assisted solvothermal reaction where 1D NRs readily assembled

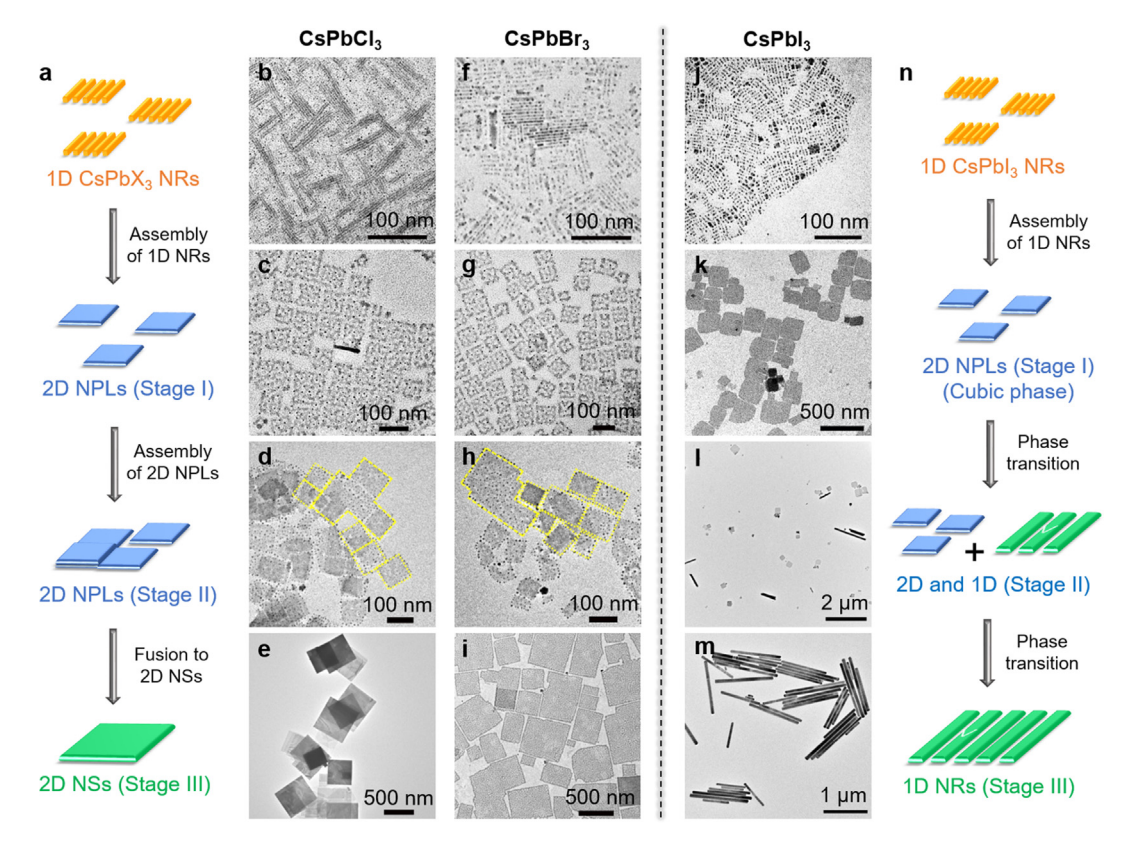


Fig. 4. (a) Schematic of the formation of 2D CsPbX₃ NPLs and NSs by the oriented attachment of CsPbX₃NRs. TEM images of (b) CsPbCl₃and (f) CsPbBr₃NRs synthesized in a three-neck round-bottom flasks under atmospheric pressure. TEM images of 2-D CsPbCl₃ NCs grown in Teflon-lined autoclaves at 160 °C for (c) 2.0 h (NPLs), (d) 2.5 h (large NPLs), and (e) 3.0 h (NSs). TEM images of CsPbBr₃ NCs grown in Teflon-lined autoclave at 160 °C for (g) 3.0 h (NPLs), (h) 4.0 h (large NPLs), and (i) 5.0 h (NSs). (j) TEM image of 1-D CsPbl₃ NRs obtained in a three-neck round-bottom flask under atmospheric pressure. TEM images of CsPbCl₃ NCs obtained after (k) 1.0 h (stage I), (l) 1.5 h (Stage II), and (m) 2 h (Stage III) grown in a Teflon-lined autoclave at 160 °C. (n) Schematic of the morphology change of CsPbl₃NCs with increasing solvothermal reaction time. (Adapted with permission from the ACS, https://doi.org/10.1021/acs.chemmater.8b01283, Ref. [88]. Further permissions related to this material excerpt should be directed to the ACS.)

at 140 °C to form laterally larger 2D CsPbBr₃ NPLs using OAm and OA as passivating ligands [97]. However, without the introduction of a mixture of ligands, they were only able to directly grow 2D CsPbBr₃ NPLs and NSs, while 2D CsPbCl₃ and CsPbI₃ were obtained with the help of anion exchange. As such, further CsPbCl_{3-x}Br_x anion alloyed NPLs were also synthesized, with a slight synthetic variance where TOPO was needed to solubilize PbCl₂ in solution.

2.4. The comparison of the current synthetic methods for 2D AIP NCs

Each of the aforementioned reaction procedures present opportunities to derive 2D perovskite NCs with their own benefits and limitations. For instance, the template mediated method discussed in Section 2.1 benefits from the acquired knowledge of reaction manipulation for 2D organic-inorganic hybrid perovskite NCs, allowing for NC assembly and synthetic exploitation prior to AIP NC synthesis. However, well established hybrid perovskite synthetic techniques must be utilized and different NCs must be first synthesized prior to the desired NC formation. This adds to the cost and complexity of the reaction, making it strenuous for further development toward industrial applications. In addition, since many direct synthetic methods are available for 2D AIP NCs, the template method is less attractive as it is currently limited to only 2D CsPbBr₃ and CsPbCl₃ NCs, which are the only NCs systems reported using the template method, to date.

The direct synthetic method discussed in Section 2.2 is by far the most simple, prevalent, and applicable for 2D AIP NC synthesis, especially 2D CsPbBr₃ NPLs. This method is bolstered by its synthetic versatility, allowing for the variance of reaction temperature, pressure, composition, and direct method to provide desired results. In addition, direct syntheses offer the most versatility including many developed advanced methods like the solvothermal method and microwave synthesis, which lead to an expanse of knowledge that can be utilized to further improved the shape control of AIP perovskite NCs. However, currently, only monodisperse 2D CsPbBr₃ and CsPbCl₃ NCs have been reported via direct synthetic approaches, where CsPbI₃NCs are rather, generally obtained by anion exchange in the presence of Cl⁻ and l⁻ anions [99,148] as current methods often result in mixed morphologies containing 1D NRs [142].

In contract, the assembly strategy under solvothermal conditions can successfully grow 2D all AIP NCs including 2D CsPbCl₃, CsPbBr₃, CsPbI₃, and CsPbBr_{1.5}I_{1.5} NCs without the assistance of anion exchange. In addition, the solvothermal step provides greater manipulability, resulting from its high-pressure nature and allow for greater NC development into more complex NC morphologies, as seen in the evolution of the as synthesized 1D NWs to 2D NPLs and then much larger 2D NSs [88]. One drawback of the assembly strategy discussed in Section 2.3 is that it requires presynthesized AIP NCs as the stock solution for the assembly of 2D AIP NCs, which adds to the complexity of the reaction. However, with the impressive versatility of the composition and morphologies of 2D AIP NCs, assembly strategies are very attractive to further advance in the field of 2D NCs.

3. A and X-site alloying

In ionic perovskites, fast ion diffusion in ABX₃ lattice make A and X- site alloying and ion exchange methods more likely to be employed [42,58,62,153–155]. Changes in the A-site normally either provides increased structural stability and photoelectric properties by incorporating Cs⁺ into a hybrid structure [45,112] to improve thermal stability or the incorporation of organic cations into all-inorganic perovskites for improved moisture stability. Generally, the stability of a ABX₃ structured perovskite can be esti-

mated according to the Goldschmidt tolerance factor (t), with a stability range of values from \sim 0.825 to 1.059 based on the Eq. (1):

$$t = \frac{r_{\rm A} + r_{\rm X}}{\sqrt{2}(r_{\rm B} + r_{\rm X})}\tag{1}$$

where, $r_{\rm A}$, $r_{\rm B}$, and $r_{\rm X}$ are the respective ionic radii of the ions in the ABX₃ perovskite structure [21,156–158]. Theoretically, the closer t is to the mid-point around ~0.942, the more stable that structure will be, as the probability of forming a stable perovskite structure drastically decreases toward the minimum and maximum limits. For example, t values for pure CsPbI₃, CsPbBr₃, and CsPbCl₃ are approximately 0.878, 0.907, and 0.914, respectively, using the corrected ionic radii values reported by Palgrave et al. [157] The resulting shift in stability between CsPbI₃ and the other two halide structures can, therefore, be understood by its close association to the bottom edge of the stability range of t at 0.825.

Manipulating the bond lengths can therefore be used to increase stability, such as by the introduction of a smaller B-site cation would decrease the average size of the B-site ionic radii, increasing the value of t closer to a more optimal range [21,159-161]. Increasing the ionic radii of the A-site as well as decreasing the radii of the X-site halide can also show increases in stability, with two distinct issues: 1) Cesium is the largest known inorganic ion capable of being implated into perovskites, meaning that any increases in radii currently has to come from the introduction of organic cations, resulting in decreased thermal stability. 2) Variances in the X-site causes drastic shifts in the bandgap of CsPbX₃ perovskites, which can negatively affect the optoelectronic properties for desired applications. For example, hybridizing CsPbI₃ NCs with other halides causes an increase in the optcial bandgap and therefore making the resulting hybridized CsPbI_{3-x}Br_x or CsPbI_{3-x}Cl_x NCs less effective in solar cell applications, even with their increased phase stability.

3.1. A-site alloying

A-site manipulation is an interesting way to vary the composition of perovskites while maintaining the original optical properties of the material. This is because small variances in the A-site have little to no effect on the NC size or the resulting optical properties, although large concentrations of A-site ions can cause lattice contraction or expansion resulting in bandgap shifts that will alter optical properties [109]. Even in these cases, the applicability of Asite alloying cannot be understated since thermodynamic and moisture stability are largely derived from the A-site composition. Compositional control in the A-site has, thus far, focused on the incorporation of alkali metal cations (e.g. Cs⁺, Rb⁺) or organic cations, such as MA and FA, in ABX3 type perovskites, with mixed results [78-82,162-164]. Most alkali metal cations are simply too small to properly support perovskite structures and thus are utilized as dopants instead, with Li⁺, Na⁺, K⁺, Rb⁺, and Cs⁺ doping being previously attempted in multiple 0D QD systems [65,109]. Yet, only the incorporation of Rb⁺ [66], FA⁺ [165], and hexylammonium (HA⁺) [167] in 2D AIP NCs has been reported to date.

As such, Sargent et al. [66], reported up to 40% Rb-alloying in CsPbBr₃ NPLs by a hot-injection method where Rb-oleate and Cs-oleate were quickly injected at the same time into a solution of PbBr₃ with OA and OAm in ODE. The resulting Rb:CsPbBr₃ QDs and NPLs showed improved stability due to decreased orbital overlap observed with tilting of the [PbBr₆] octahedral structure. The QD and NPL syntheses only varied according to the ligand concentration, where the QD synthesis used a 1:1 v:v ratio and the NPL synthesis used a 2:1 v:v ratio of OA-to-OAm, respectively [66]. When applied to perovskite LED systems, the OD QDs outperformed the 2D NPLs with resulting external quantum efficiencies

of 0.87% and 0.11%, respectively. A decreased PL QY and external quantum efficecy was observed with the 2D NPLs over the 0D QDs, likely due to the increased surface-to-volume ratio of the NPLs that would therfore cause an increase in surface traps states following excessive cleaning [66].

Deng et al. [165], developed a facile hot-injection method by the rapid introduction of Cs-oleate and FA-oleate precursors, at the same time, into a solution of PbX_2 (X = Br, I, or mixture thereof) with OAm, OA, and on occasion bis(2-ethylhexyl)amine in ODE to synthesize 33% FA-alloyed CsPbBr_{3-x}I_x NWs and NSs. It was found that ligand composition had a large role in the NC morphology with an acid rich (3.4:1.4 OA-to-OAm v/v ratio) environments resulting primarily in the formation of NSs, whereas amine rich (1.4:3.4 OA-to-OAm v/v ratio) environments resulted in the formation of NWs. Notably, iodine rich compositions (FA:CsPbBr_{0.5}I_{2.5} and FA:CsPbI₃) resulted in NW formation even in acid rich conditions. Nanocrystal stability was also tested to represent the structural improvements made by FA+ introduction for iodine rich CsPbBr_{0.5}I_{2.5} and FA:CsPbBr_{0.5}I_{2.5} NWs. After 2 h of irradiation using a 420 nm UV-vis laser in two separate mixtures of hexane with acetone and hexane with ethyl acetate to purposefully degrade the NCs. The non-alloyed sample degraded to a much greater extent than the FA-alloyed sample with only ~2% remaining PL after 2 h of testing in both the hexane-ethyl acetate and hexaneacetone solutions. Meanwhile, the FA-alloyed sample maintained 70% and 5.3% of its original PL after 2 h of testing in the hexaneethyl acetate and hexane-acetone solutions, respectively [165]. Shape and composition control in these structures with the increased stability highly aid them in possible future optoelectronic applications in light emitting devices and detection.

Incorporation of organic cations into AIP introduces new properties as well as to increases resistance to hydrolysis in high moisture environments. Such as the case by Miyasaka et al. [124], where they showed that A-site incorporation of MA and FA as an alloy can increased moisture stability but decrease thermal stability in 2D layered Ruddlesden-Popper (RP) Cs₂Pbl₂(SCN)₂ films. This likely stems from the much larger nonpolar bodies of MA and FA being intrinsically less reactive with water, vet more susceptible to thermal degradation than Cs⁺. Interestingly, the incorporation of SCN⁻ as an anion in ABI₃ lattice could increase thermal stability (as discussed below in Section 3.2) [124]. Halpert et al. [166] and Jin et al. [167] further showed the manipulability of 2D RP perovskites by A-site alloying with organic cations. Butylammonium (BA⁺) was used in an alloying method with CsPbBr₃ NSs to cause the formation of $(BA)_2Cs_{n-1}Pb_n(Br/Y)_{3n+1}$ (Y = Cl, I) RP NSs, where the NS thickness was controlled based on BA+ concentration [166]. Increased concentrations of BA⁺ create more separations between RP layers therefore producing thinner NSs, with lower concentrations resulting in the combination of RP layers into thicker NSs. This reaction followed a spin-coating method where the NSs were formed following thermal evaporation of the perovskite precursors on the substrate layer [166]. Additionally, the NSs grew at a preferential orientation perpendicular to the substrate, favoring charge transport and separation in the solar cells, which lead to a 4.84% power conversion efficiency of LED device. The device consisting of FTO/TiO₂/BA₂CsPb₂I₇/spiro-OMeTAD/Au was also significantly more stable than its CsPbI₃ counterpart, maintaining 92% of its overall power conversion efficiency after aging for 30 days under ambient conditions [166].

Jin et al. synthesized a wide variety of hexylammonium (HA⁺) A-site alloyed RP NPLs through a room temperature colloidal reaction under ambient conditions [167]. This method was used to test the effects of A-site size on the optoelectronic properties of the resulting NPLs, specifically with applications in solar cells. The resulting (HA)₂CsPb₂I₇ NPLs presented the highest PL QY at 11.5% with a general trend showing that increased A-site size from Cs

to acetamidinium produced decreased PL QY and lifetime decay. Adversely, the performance of the resulting solar cell increased with A-site size, likely caused by increased thin film passivation with the larger A-site ions [167].

3.2. X-site alloying

The most basic form and likely most heavily utilized forms of manipulation, especially for optical properties, is through alloying and complete ion exchange of the X-site anion in ABX₃ perovskites, where the halide composition of the perovskite NCs can be reversibly changed between Cl, Br, and I. The anion determines the crystals' relative size, bandgap, as well as the overall stability. On one hand we have large bandgap materials like CsPbCl₃ and CsPbBr₃ and on the other, small band-gap materials like CsPbI₃, with the smaller bandgap making iodine-based perovskites highly sought after for solar cell technology. However, stability issues have kept the use of CsPbI₃ to a minimum, therefore forcing researchers to instead form X-site alloyed AIP NCs, while attempting to maintain NC stability and the optical properties of CsPbI₃. Multiple recent studies have shown the incorporation and exchange of Cl and Br into iodine based 2D AIP with spectrum blue shifts in the resulting optical properties [74,120,122,123,168,169]. One such report by Zhu et al. [120] showed that by exchanging halide ions, the structure of the resulting crystal could be manipulated from 1D NRs into 2D NCs (Fig. 5a) along with the normal shift in the optical emission spectra. By increasing iodide content in a mixed halide CsPbBr_{3-x}I_x NC, the structure could be tuned from NRs to NPLs along with a continuous red-shift in the emission from 464 to 667 nm (Fig. 5b) and compositional shift observed in the XRD while maintaining a cubic structure (Fig. 5c) [120]. When utilized for LED applications these NCs observed a tunable correlated-color temperature range from 2513 to 9783 K. Under optimized conditions, a color rendering index of 95 was achieved, indicating that the white light emission is a near faithful comparison to ideal or natural light sources.

Methods of inducing a more stable structure while maintaining the optical properties of iodine containing perovskites has now progressed to the use of halide-like ions such as thiocyanate (SCN⁻). Recent reports by Chueh et al. [123] and Miyasaka et al. [124] have shown that SCN⁻ introduction can increase thermal stability in $Cs_2Pb(SCN)_2X_2$ (X = Br, I, and mixture thereof) and $CsPbI_2$ (-SCN)₂ AIP NCs, respectively. However, SCN⁻ incorporation does not affect the optical emission position such as with common ion exchange methods, resulting in more stable NCs without changing the material's band-structure. In addition, optical quenching effects were observed with SCN⁻ incorporation. On the other hand, the rod-like shape of SCN⁻ actually assists in the formation of 2D structures by providing a template like structure by which the NCs can grow. Chueh et al. showed that the incorporation of SCNincreased environmental stability in RP phase 2D perovskites, with CsPb(SCN)₂I₂ displaying the most impressive optical response in comparison to the other pure halide and mixed halide samples tested [123]. The SCN⁻ ions did not interfere with further anion exchange of the site either, rather allowing for the incorporation of multiple ions to form mixed halide structures. Miyasaka et al. also showed a large increased in thermal and structural stability with SCN⁻ introduction in all-inorganic RP perovskites, in comparison to pure Cs₂PbI₄ NCs [124]. However, they found that stability in high moisture environments decreased since the SCN- acts as a π -acceptor pulling electron density away from Cs⁺, therefore making Cs⁺ more likely to by hydrolyzed in the presence of water. In this work, perovskites doped or alloyed in the A and B-sites with SCN⁻ incorporated in the X-site were also tested for stability but resulted in less thermally stable structures than the Cs₂PbI₂(SCN)₂ structure.

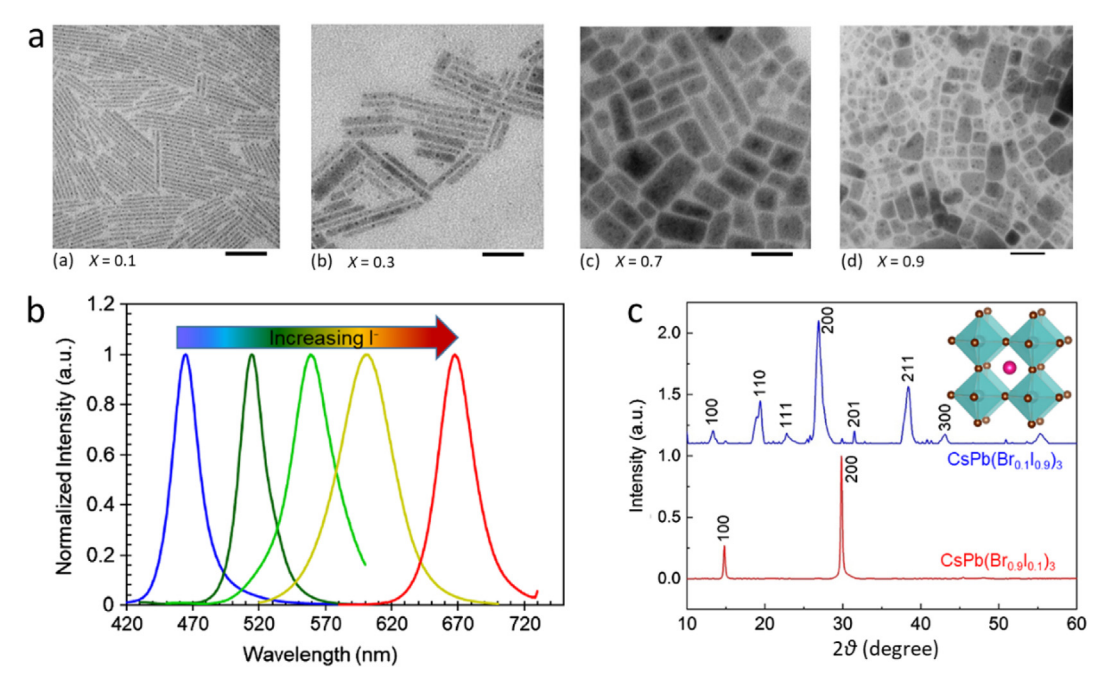


Fig. 5. (a) TEM images of CsPb(Br_{1-x}I_x)₃ (x = 0.1, 0.3, 0.7, 0.9) NCs, where the scale bar is 50 nm for each, and (b) Normalized emission spectra (x = 0, 0.4, 0.6, 0.7, 0.9) left to right, respectively) with respect to iodine halide composition. (c) XRD for CsPb(Br_{1-x}I_x)₃ (x = 0.1 (red), 0.9 (blue)). Inset represents a general cubic crystal structure for cubic CsPbX₃ NCs. Adapted from Ref. [120] with permission from the OSA publishing group.

4. B-site doping

Dopant incorporation in 2D AIP NCs is primarily performed in the B-site, which offers extensive synthetic control over the composition of the resulting NCs. Due to the importance of the B-site to the resulting optical properties and the structural stability of perovskites, dopant incorporation has been widely studied in perovskite nanocubes and other similar highly confined NC systems to manipulate the resulting NC properties. However, B-site doping in 2D AIP NCs is still regarded as a difficult process due to the high formation energy for cation vacancies and a lack of the interstitial sites necessary for fast ion diffusion [58,153]. Additionally, large size disparity between Pb²⁺ (133 pm) and most B-site dopants, such as Mn²⁺ (97 pm), could lead to large lattice strain due to dopant incorporation, making high concentration doping difficult [50]. Therefore, the doping efficiency can be rather low even with very high concentrations of dopant precursor introduced in the synthesis [50,64,170]. For example, Parobek et al. obtained 0.2% doping in CsPbCl₃ nanocubes by using extremely high concentrations of Mn precursor with a Mn:Pb in a 3:2 mol ratio [170].

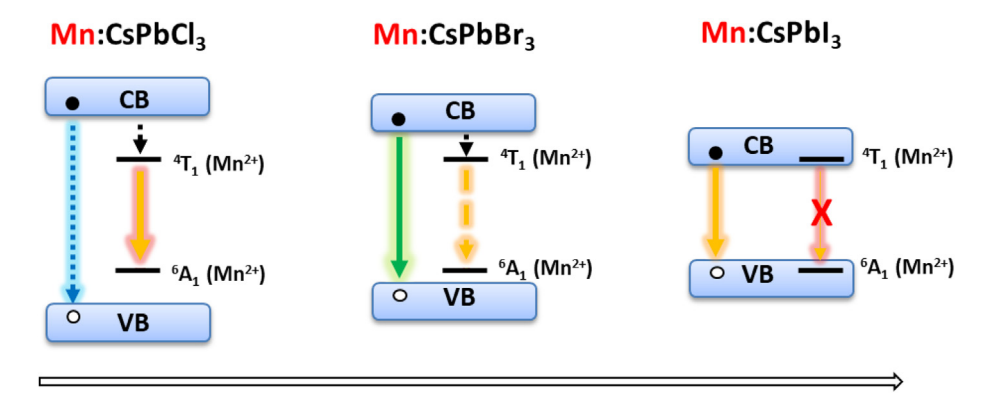
Manganese ions (Mn²⁺), as the most prevalent dopant in 2D AIP NCs to date, has been of massive interest for over a decade for doped metal chalcogenide and perovskite NCs because of its d electron energy levels within the bandgap of many semiconductor NCs. Therefore, host NCs to dopant energy transfer can produce a strong dopant emission. Additionally, the 5/2 spin state of Mn²⁺ can introduce interesting magnetic properties into host NCs from isolated magnetic dopants as well as magnetic coupling between magnetic Mn center, which are useful for spintronic applications [171–177].

So far Mn-doped AIP studies focus predominantly on the CsPbCl₃ host lattice because it has a wide bandgap that easily transfers energy to dopant orbital, with many reports showing the orange Mn photoluminescence (PL) (Scheme 2). However, B-site Mn-doping in CsPbBr₃ has proven much more difficult, providing either weak Mn PL or lacking dopant emission entirely. Many theories have been proposed to explain the lack of a strong Mn²⁺ emission, including difficulties with incorporation due to the high

stability of CsPbBr₃ not allowing for dopant incorporation, the variance in bond dissociation enthalpies between dopant precursors and the host lattice, as well as the close band alignment between the conduction band of CsPbBr₃ and the ⁴T₁ d-state of Mn²⁺ [56,63,68,72,73] (Scheme 2). Additionally, the introduction of Mn²⁺ into CsPbI₃ does not offer much in terms of improved optical properties, due to its small bandgap of CsPbI₃, and thus is not normally studied in Mn doped systems (Scheme 2). It should be noted that, however, Mn doping can affect the stability of OD CsPbI₃ NCs. Manna et al. [57] demonstrated that Mn²⁺ incorporation in CsPbI₃ NCs resulted in increased phase stability in both NC films and in solution, causing maintained phase stability for over a month. As such, Mn-doping in CsPbI₃ will be largely unexplored in this section and we will be discussing the CsPbCl₃ and CsPbBr₃ host NCs separately in Section 4.1 and in Section 4.2, respectively.

4.1. Manganese doped 2D CsPbCl₃

The Nag group showed the first instance of Mn doping in 2D CsPbCl₃ NPLs using a facile room temperature reaction [68]. In a typical reaction, a mixture was prepared containing a Csprecursor, preheated to 100 °C, ODE, OA, and OAm, followed by the rapid injection of a PbCl₂ precursor containing different Mn² concentrations to study variances in the host-to-dopant energy transfer of the resulting doped NPLs. Increased in the Mn doping concentration (up to 2% [Mn]) resulted in increased host-todopant energy transfer, and a red-shift from the host emisison at ~360 nm to a Mn emisison at ~586 nm. However, concentrations greater than 0.8% resulted in decreased Mn PL due to short range Mn-Mn interactions. Additionally, Mn doping can significantly increase PL QYs of the NPLs from 2.8% for the undoped NPLs to the highest PL QY at 20.3% for 0.8% doped NPLs. Mn doped CsPbBr₃ NPLs were also synthesized through an anion exchange method as the direct synthetic results were "not promising", likely due to the increased stability of the CsPbBr₃ lattice causing greater difficulty with B-site dopant incorporation, resulted in a weak Mn PL [68].



Decrease in bandgap, less host-to-dopant energy transfer

Scheme 2. Schematic detailing the changes in bandgap between CsPbCl₃, CsPbBr₃, and CsPbl₃ NCs, resulting in reduced host excited electrons to Mn dopant energy transfer and therefore singnifiant Mn PL can be obsterved in Mn:CsPbCl₃ with a large bandgap, while weak or no Mn PL in Mn:CsPbBr₃ with a moderate bandgap and no Mn PL in Mn: CsPbI₃ with a small bandgap.

Recently, our group developed an efficient doping strategy for Mn doped 2D CsPbCl₃ NPLs through a post-synthetic solvothermal process to overcome the limitations of B-site doping (Fig. 6a and b) [67]. In the first step, we synthesized lightly doped 2D Mn:CsPbCl₃ NPLs (~1.0 % [Mn], mol% to Pb) by the injection of Cs-oleate into an OA and OAm solution containing PbCl₂ and MnCl₂ (80%, mol% to Pb) at 120 °C. Then, the stock solution was transferred into a Teflon-lined stainless-steel autoclave to grow heavily doped CsPbCl₃ NPLs (up to 16.8%) under solvothermal condition at 160-200 °C for 2-5 h. While the original lightly doped 2D Mn:CsPbCl₃ NPLs were obtained from growth doping, higher Mn doping efficiencies were achieved through diffusion doping under pressuremediated solvothermal conditions, resulting in enhanced Mn PL (Fig. 6c). The increased doping concentration could lead to higher Mn PL QYs and stronger Mn-Mn interactions. Surprisingly, a new CsMnCl₃ phase with complete dopant substitution by spinodal decomposition was observed with extended solvothermal treatment, which is confirmed by powder X-ray diffraction (XRD) (Fig. 6d), X-ray absorption near edge spectroscopy (XANES), and electron paramagnetic resonance (EPR) (Fig. 6e). The ability to incorporate a new phase by spinodal decomposition provides a new understanding of doping inside 2D AIP NCs and a promising approach to study the interactions between the impurity and the host under moderate temperature and pressure.

In addition to the ligand composition tuning methods developed by Manna [102] and Zheng [88] for 2D AIP NCs, a later publication by Tang et al. [70] found that by manipulating ligand concentration under similar solvothermal conditions, nanocubes and NPLs can be synthesized, with lower concentrations of OAm and OA ligands preferring to form 2D CsPbCl₃ NCs. It was also determined that by utilizing more mild solvothermal conditions (i.e. at 120 °C), NPLs doping concentrations could be increased, from ~6% to 25% [Mn] to total spinodal decomposition to CsMnCl₃, without inciting large scale NPL stacking to form larger 2D NCs [70].

Interestingly, Lin et al. showed that multiphoton absorption can be realized in 0.2% Mn-doped 2D CsPbCl₃ NCs similar to upconversion effects shown in lanthanide doped NCs (Fig. 7) [71]. The 680 nm fs pulses cause bandedge excitation via a two-photon absorption process followed by host-to-dopant energy transfer and a Mn PL at ~600 nm (Fig. 7a and 7b), while the significantly lower energy 1300 nm fs pulses lead to direct Mn²⁺ excitation throught a three-photon absorption process (Fig. 7c and d). The two- and three-photon absorption cross-sections of 2D Mn: CsPbCl₃ NPLs were 1237 GM/nm³ and 2.24 \times 10⁻⁷⁸ cm⁵ •s² • photon/nm³ in the visible light and biological windows, respectively,

which were increased by 6.8 and 7.2-fold in comparison to corresponding 0D perovskite nanocubes (normalized to volume) (Fig. 7a and c).

4.2. Manganese doped 2D CsPbBr₃

While Mn can be doped inside CsPbCl₃ NCs with intense Mn PL reported in many cases, doping inside CsPbBr₃ has been proven challenging. One possible reason is the large separation between the dissociation energies of PbBr₂ (249 KJ/mol) and MnBr₂ (314 KJ/mol) in comparison to PbCl₂ (301 KJ/mol) and MnCl₂ (338 KJ/mol), impeded Mn introduciton into the CsPbBr₃ lattice due to the higher bond stability of MnBr₂ than PbBr₂ [72]. Furthermore, Klimov et al. showed that this issue could be further compounded by forming a Mn-oleate complex for dopant introduction, which results in a Mn-O (402 KJ/mol) bond that is significantly more stable than the PbBr₂ (249 KI/mol) bond [56].

Nag et al. tested the disparity between different dopant precursors using a post-synthetic doping method on CsPbBr3 NPLs (Fig. 8a) [73]. Their method involves first synthesizing CsPbBr₃ NPLs, followed by the treatment of the resulting NPLs with a MnBr₂ precursor dissolved in a 1:3 mixture of acetone to toluene by volume. This solution is optimal to dissolve MnBr₂ while not providing enough acetone to destabilize the NPLs. Superior synthethic control with the use of MnBr₂ as a precursor resulting in increased Mn incorporation and Mn-emission intensity, in comparison to the Mn-oleate and HBr acid assisted Mn-oleate methods (Fig. 8b and c) [73]. They also provided a simplified post-synthetic method for both up to 6.5% Mn²⁺ and 1.4% Yb³⁺ introduction in monodispersed CsPbBr₃ NPLs, while also illucidating the mechanism as to why the 2D NPLs have a larger host-to-dopant energy transfer than the 0D Mn-doped CsPbBr₃ NCs. It was determined that the ⁴T₁ orbital of Mn and the conduction band of CsPbBr₃ are close enough in energy to result in a thermally activated back energy transfer from the dopant to the host even though the d-d transitions of Mn²⁺ lies within the bandgap of CsPbBr3. Therefore, an increased intensity and continuously red-shifting of the Mn emission at lower temperatures in CsPbBr₃ NCs was observed [73]. This also explains why thin 2D Mn:CsPbBr3 NCs have a more intense Mn emission as the increased quantum confinement increases the CsPbBr₃ bandgap, therefore making the back energy transfer at room temperature less likely (Fig. 8d) [73].

To combat the disparity in bond stability between MnBr₂ and PbBr₂, Son et al. [72] developed a two step reaction mechanism involving the creation of an, up to \sim 11%, Mn-doped L₂[Pb_{1-x}Mn_x] Br₄ intermediate followed by the injection of a Cs-oleate precursor

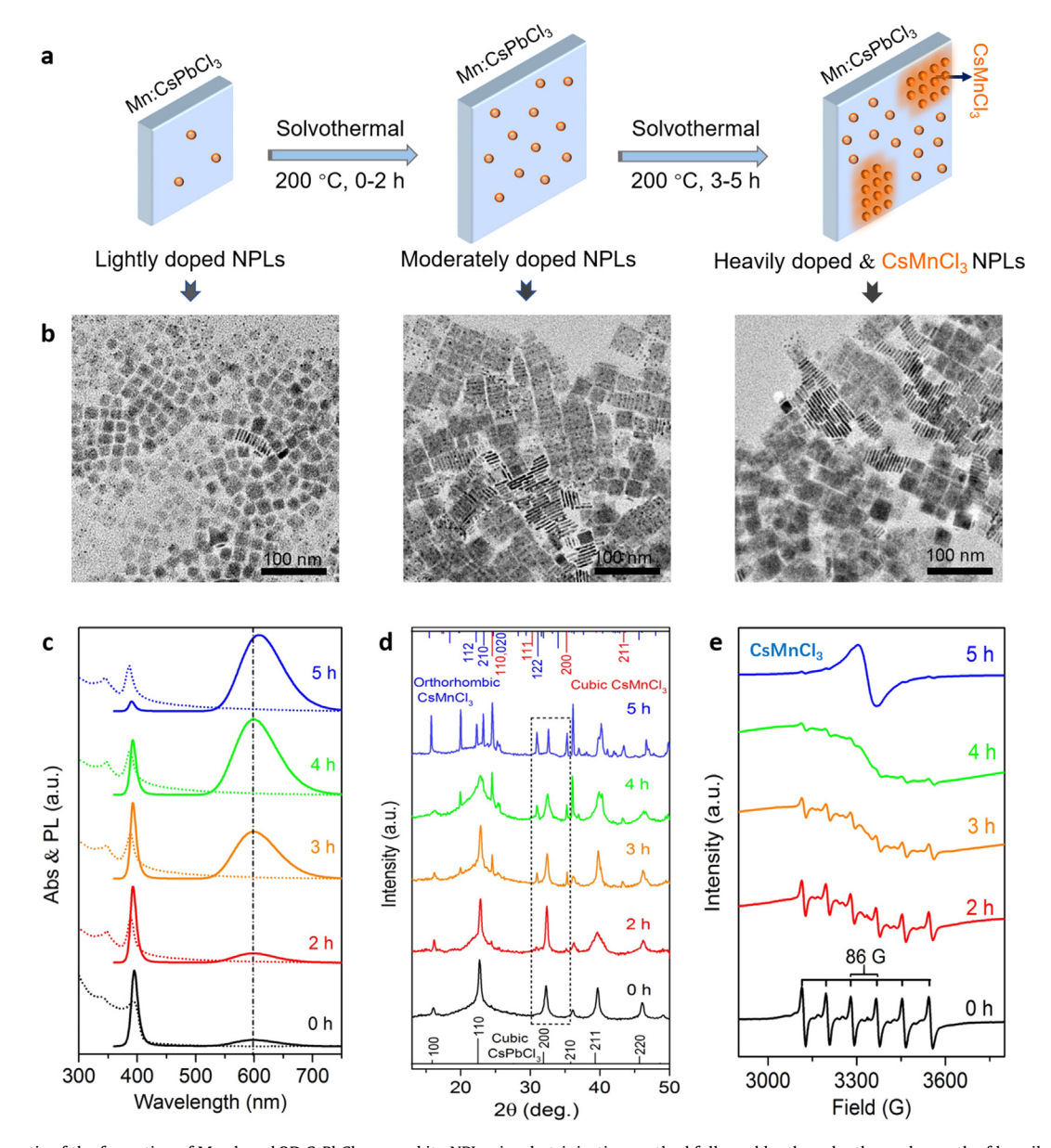


Fig. 6. (a) Schematic of the formation of Mn-doped 2D CsPbCl₃ perovskite NPLs via a hot-injection method followed by the solvothermal growth of heavily larger Mn-doped CsPbCl₃ NPLs and CsMnCl₃ inclusion after phase segregation. (b) TEM images of corresponding small 2D Mn:CsPbCl₃ perovskite NPLs synthesized in three-neck round-bottom flasks and larger 2D Mn:CsPbCl₃ perovskite NPLs grown in Teflon-lined autoclaves after solvothermal treatments. (c) Optical properties, (d) XRD patterns, and (e) Room temperature X-band EPR spectra of 2D Mn:CsPbCl₃ NPLs (using 80% Mn as precursor, mol% to Pb) under different solvothermal treatment time. (Adapted with permission from the ACS, https://doi.org/10.1021/acs.chemmater.8b02657, Ref. [67]. Further permissions related to this material excerpt should be directed to the ACS.)

that results in the production of 0D Mn:CsPbBr₃ NCs and, up to ~2% Mn-doped, 2D CsPbBr₃ NPLs that are easily separable by centrifugation. The intermediate complex is necessary for the synthesis of doped CsPbBr₃ NCs to avoid directly breaking the MnBr₂ bond. Despite the incorporation of Mn²⁺ into the CsPbBr₃ NC lattice and the the fact that the CsPbBr₃ bandgap is large enough to contain the d-d statesof Mn²⁺, only a weak Mn PL was obtained in the 0D NC system, while the thin 2D NPLs with a bigger bandgap resulted in an increased host-to-dopant energy transfer and a more intensed Mn PL [72].

4.3. Manganese doped Ruddlesden-Popper NCs

Ruddlesden-Popper $(Cs_{n+1}Pb_nX_{3n+1})$ perovskite NCs are a newly emerging perovskite subclass that has only recently been produced on a nanoscale. These materials are currently of interest due to their interesting layered structure, which forms as individual

CsPbX₃ layers separated by CsX spacing layers [178]. This structure causes increased quantum confinement due to the individual structures acting near-independently, resulting in an increased bandgap and a subsequent optical blue-shift. Unfortunately, the RP structure is highly unstable and normally only presents very low PL QY below 1% as pure RP NCs [168,178,179]. Therefore, Mn²⁺ doping has been of interest in these systems as a means to improve PL OY while maintaining the RP phase. However, it should be noted that recent report by Biswas et al. showed that by introducing PbBr₂ or MnCl₂ post-synthetically into the as synthesized Cs₂PbI₂Cl₂ NPLs, the 2D NPLs can be tuned to 3D CsPbBr₃ or 0D Cs₄-PbCl₆ NCs, respectively [178]. It is therefore imparative that dopant incorporation is controlled as to not cause undesired shifts in morphology. Similar effects were reported by Pradhan et al., where reactions that failed to form RP phase 2D perovskites rather formed diverse 3D CsPbX₃ and 0D Cs₄PbX₆ products instead, with X determined by the original reaction composition [74].

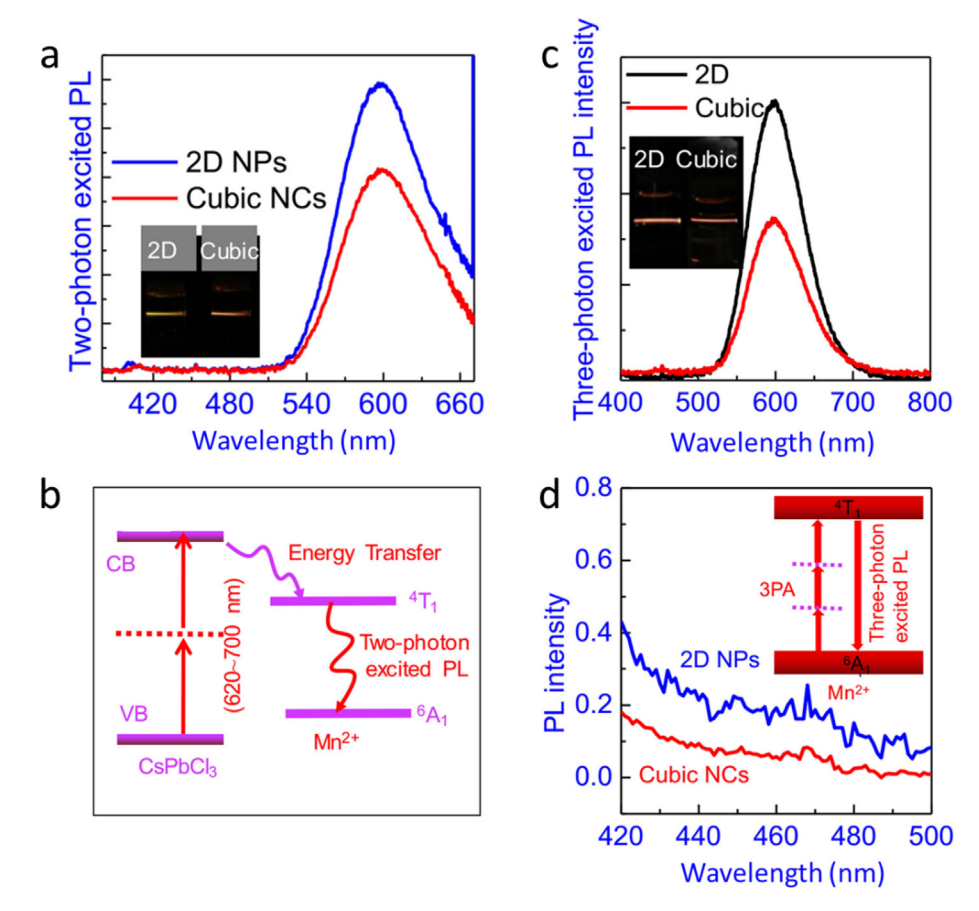


Fig. 7. PL spectra of Mn:CsPbCl₃ 2D NCs and nanocubes excited by (a) 680 nm and (c) 1300 nm fs pulses. Schematic representation of the energy transfer pathway for (b) two-photon and (d) three-photon linear absorption spectra of Mn:CsPbCl₃ 2D NCs and nanocubes. Adapted from Ref. [71] with permission from the OSA publishing group.

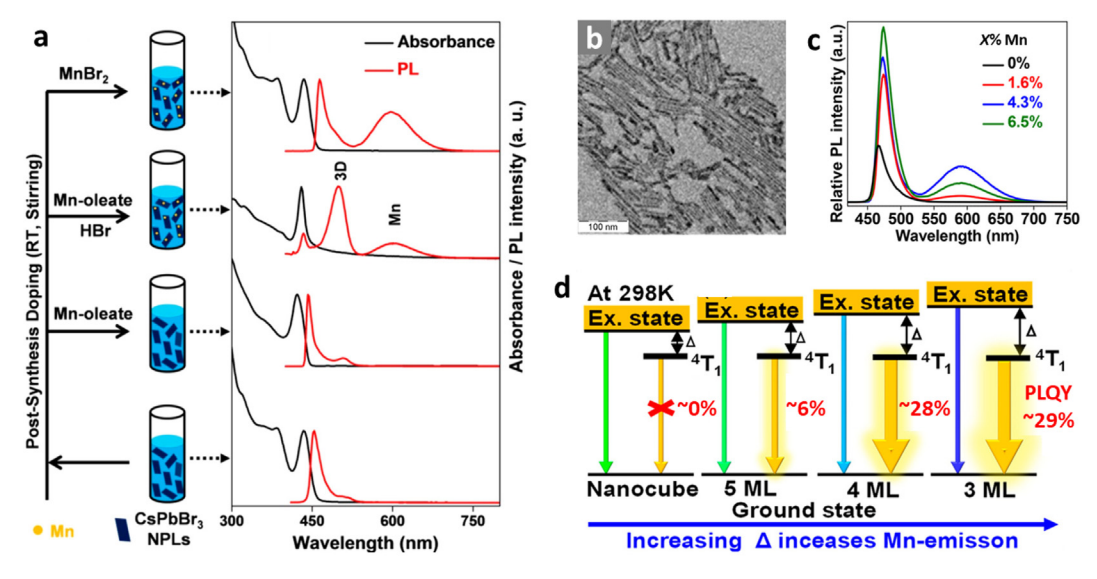


Fig. 8. (a) Schematic showing the post-synthetic doping of Mn²⁺ into CsPbBr₃ NPLs with different Mn precursors and the representative absorbance (black) and PL (red) spectra from the resulting products for each corresponding dopant precursor. (b and c) Data corresponding to 5 ML Mn:CsPbBr₃ NPLs, where (b) is a TEM image of 4.3% NPLs, and (c) is the PL spectra of the resulting doped NPLs with respect to dopant concentration. (d) Schematic detailing the changes in bandgap between Mn:CsPbBr₃ NCs and Mn: CsPbBr₃ NPLs of decreasing thinknesses from 5 to 3 unit cells, left to right respectively, resulting in reduced back energy transfer and therefore a more intense Mn PL. (Adapted with permission from the ACS, https://doi.org/10.1021/acs.chemmater.8b03066, Ref. [73]. Further permissions related to this material excerpt should be directed to the ACS.)

Pradhan et al. did, however, suceed in developing the first doped 2D RP perovskite NC synthesis for tetrogonal phase Mndoped Cs₂PbCl₂I₂ NPLs following a hot-injection synthesis where

an OAm-HCl + OAm-HI precursor is injected to a mixture of a Mn-acetate, Cs_2CO_3 , PbO, and ligand solution at 180 °C [74]. The resulting NPLs presented a strong Mn d-d transition, while also

increasing the host PL causing an amplified PL QY from below 1% to ~16% with 1.7% Mn²⁺ incorporation. Interestingly, Feldman et al. found that they could induce RP phase planes in CsPbCl₃ NCs NC by incorporating Mn²⁺. With increasing dopant concentrations, from 0.5 to 3%, more RP planes resulted as defect like layers, causing a blue-shifted and broadened host emission [180]. The reaction followed an ultrasonication method where PbCl₂, MnCl₂, Csacetate, OA, and OAm are directly sonicated, resulting in the formation of Mn-doped CsPbCl₃ NCs.

4.4. Additional dopant ions for 2D AIP NCs

While not largely prevalent in 2D AIP NCs as of yet, there are still multiple other dopant ions that have been reported for Bsite doping, such as Yb³⁺, Sb³⁺, Sn²⁺, and Ni²⁺, that provide interesting functionality to perovskite NCs. For example, Yb3+-doping in 2D AIP NCs was demonstrated in CsPbBr₃ NPLs by Nag et al. [73] by a post-synthetic method involving the treatment of the as synthesized CsPbBr₃ NPLs with Yb(NO₃)₃ in a methyl acetate and toluene solution. The resulting 1.4% Yb-doped CsPbBr₃ NPLs expressed a strong host emission at ~440 nm and an Yb3+ emission at ~982 nm with a lifetime decay of ~400 μ s [73]. Murali et al. [75] further illucidated the effects of doping on PL properties of Nidoped CsPbBr₃ 2D NPLs. It was reported that Ni-doping improved non-linear optical susceptibilty from 3.0×10^{-10} to 7.0×10^{-10} esu at 0.05 to 0.08% [Ni], and the two-photon absorption cross section from 1.6×10^4 to 4.1×10^4 GM at 0.08 to 0.1% [Ni] [75]. The increase in two-photon absorption cross section and non-linear optical susceptibility were both attributed to localized surface plasmon-induced charge transfer effects that occurs at the interface between the metal and semiconductor [75].

Pradhan et al. [77], on the other hand, showed that the introduction of large equivalents of Sb³⁺ (>10%) caused anisotropic growth of otherwise OD NCs into 2D NPLs by a hot-injection method, in which Cs-oleate was rapidly injected into a 1:2 mol% ratio mixture of SbI₃ and PbI₂ in ODE. It was reported that Sb³⁺ incorporation increased the stability in the corresponding CsPbI₃ NCs, tested in a NC film, resulting in maintained cubic phase stability for over a month under ambient conditions [77]. Sb:CsPbI₃ NCs were further explored for photovoltaic applications in solar cells resulting in a maximum efficiency of 9.4%. Similarly, Yang et al. [76], showed that Sn²⁺ incorporation in a hot-injection synthesis could assist in the formation of 2D CsPbBr3 NPLs. The synthesis involved the rapid injection of Cs-oleate into a mixture of PbBr₂ and SnBr₂ with OA and OAm in ODE at temperatures ranging from 105 to 150 °C. Relatively low temperatures were utilized to resist the oxidation of Sn²⁺ to Sn⁴⁺, with 135 °C and 3.4% Sn²⁺ incorporation being the optimized reaction conditions for monodispersed Sn:CsPbBr₃ NPLs of 7.2 nm lateral dimensions and 2 nm thickness. Further analysis demonstrated that Sn²⁺ incorportation improved photodetectiveity in a perovskite-based Sn:CsPbBr3:polymethyl methacrylate photodetector. Sn²⁺ was found to assist in the formation of interfacial traps between the perovskite layer and [6,6]phenyl-C₆₁-butyric acid methyl ester (PC₆₀BM) layer, resulting in detectivities on the order of 1011 Jones when excited using UVlight from 310 to 400 nm under a -7V reverse bias [76].

5. Applications of 2D AIP NCs

While the impressive properties of 2D AIP NCs, the development and application of these materials is currently lacking to a near extreme. 2D AIP and doped AIP NCs have not been of exceptional use for LED, solar cell, and lasing applications, to date. So far 0D perovskite QDs have been used for LED and solar cell applications due to their improved stability and typically higher PL QY

[181–183], as well as 1D NRs for lasing applications as they have a larger anisotropic influence on their emission than NPLs have currently shown [184–186]. Layered 2D RP perovskites are promising materials for light emitting applications, due to their flexible composition and structural tunability making them useful for LED applications [166,187]. While these structures tend to be relatively stable in comparison to 2D hybrid perovskites, they are still well into their infancy in terms of utility and require significantly more attention before they will be properly useful for real-world applications [15,187,188].

So far, 2D AIP NCs have primarily been of interest for transistor applications, due to their distinct advantage in the production of flexible optoelectronic devices, ability to create large-area crackfree films, higher in plane carrier mobility, longer diffusion lengths, longer lifetimes, lack of grain boundaries, and improved electron transport [11,19,189–191]. However, a few key issues still remain for perovskite NCs toward transistor applications including, limited charge transport, surface ligand interference, as well as the limited stability of perovskite NCs that hinder applicability. Doping and alloying are possible solutions to the aforementioned issues that limit 2D NC application in real world devices. Primarily, heterovalent B-site doping is one possible method to ease ion migration while improving charge transport. Meanwhile, surface doping or complex surface encapsulation/decoration is another potential method for mitigating surface ligand interactions while improving direct device processability and stability. The stability of the 2D AIP NCs as well as the corresponding devices will be discussed in the Conclusions and Perspectives section of this review.

5.1. Charge transport applications

One of the most prominent issues of charge transport in perovskite-based devices is the A- and X-site fast ion migration that can result in ion accumulation at the interface between the perovskite layer and surrounding dielectric materials, impeding perovskite electron transport performance and ion mobility [192]. This is especially problematic in photodetector and solar cell applications as both heavily rely on charge carrier generation/separation, carrier transport, and carrier collection by electrodes. Which is important due to the wide applicability of photodetectors in light communication, image sensing, and other fields that need photoelectric conversion ability. Therefore, improving electron transport and ion mobility by reducing ion migration is a key issue, especially since ion migration cannot be suppressed by encapsulation. Compositional tuning can suppressing ion migration, by introducing inorganic A-site cations over the previously utilized organic cations, whose decreased volatility made them far more applicable for room temperature transistors [192]. For example, the replacement of organic cations with Cs⁺ inorganic cations for room temperature AIP transistor applications, resulted in a moderate hole mobility of 0.32 cm² V⁻¹ s⁻¹ without any metal electrode or dielectric modifications [193], which exceeds hybrid NCs for transistor applications due to the decreased ion migration and ion screening effects achieved when utilizing Cs-based perovskites.

In ideal AIP NPLs, no internal grain boundary along the lateral direction exists, ensuring good charge carrier transport in laterally layered electrical devices and minimizing exciton quenching in optical applications, which could exceed the positive influence of using extremely thin perovskite films containing 0D NCs. Furthermore, 2D NCs enable improved optoelectronics by their scalable fabrication and improved control over NC growth and transfer for device fabrication [19]. For example, AIP 2D CsPbBr₃ microcrystals have been shown capable of bridging individual 2D microcrystals across a transistor channel with no extrinsic grain boundaries among the neighboring microplates [193]. These same microplates demonstrated a clear field-effect of the drain current regulated by

the gate voltage through field-effect transistor (FET) analysis, which correlates to improved transistor applicability in comparison to 2D hybrid NC systems [193–196]. Furthermore, applying 2D AIP NC films, in the form of CsPbBr₃ NS films, in a photodetector device resulted in a short rise and decay time of 0.019 or 0.025 ms, which is significantly shorter than rise and decay times that have been demonstrated by 2D hybrid perovskite photodetectors [197].

Alloying approaches through the A- and X-sites of the ABX₃ general crystal structure have shown little utility toward resolving issues with ion migration and ion accumulation. Alloying within the A-site either offers smaller metal cations or organic ions and would therefore not play much of a role in this issue, as the introduction of organic and small inorganic cations would increase ion migration. X-site alloying could be used to further stabilize the structure or tune the NC bandgap/optical properties but does not play a large role in electrical properties, at least not to date. There is simply not enough work outside of halide exchange to demonstrate the promising applicability of the X-site ions toward the reduction of ion migration. Consequently, B-site doping is the most likely method for improving charge transport while also reducing ion migration, primarily through the introduction of heterovalent ions. Heterovalent B-site doping offers a method to improve ion transport through the development of ion vacancy channels within the perovskite NCs, further adding to the already near ideal charge transport properties of 2D AIP NCs [49,54,198]. Afterall, Bi³⁺ doped CsPbI₃ NCs showed applicability for NIR luminescent materials with huge potential for applications in telecommunications, however, Bi did not provide the necessary structural stability to make the CsPbI₃NCs truly applicable [199]. Current synthetic reports on 2D AIP NC doping with heterovalent ions is limited, however, of these reports, the increased PL QY resulting from Yb³⁺ [73] and the increased stability offered by Sb³⁺ [77] offer unique opportunities for future optoelectronic applications.

5.2. 2D AIP device interface engineering

It should be noted that the NPL/dielectric interface can be of vital importance in a transistor platform. In fact, the few nanometer thin layer NPL/dielectric interface controls the field-effect conductivity for the entire transistor channel [200], which has become an issue with solution-processed 2D NCs as organic residues and surface ligands are currently suspected of hindering field-effect transistor (FET) applicability. For example, colloidal CsPbBr₃ NPLs have been shown to exhibit excellent photosensitivity in photodetector applications that contain two metal electrodes, however, applying a third electrode to the back gate does not allow for room temperature field-effects [201]. On the other hand, CVDsynthesized CsPbBr₃ NPLs exhibit both excellent photosensitivity and room temperature field-effects, demonstrating that the issue is likely surface ligand related [193,202]. However, the effects of surface ligands on FET and photodetector applicability requires further study to provide a greater understanding of the exact ligand effects.

There are a few methods of surface treatment that could prove useful with delaying surface ligand interference. For example, 2D boron nitride can be used as an encapsulating layer for a heterojunction photodetector based on graphene/perovskite composites [203]. These types of heterojunctions are utilized to improve film stability, improve ion mobility, and to act as protective layers against device overlap leading to decay. Properly passivating 2D perovskite NCs with other component layers, such as BN or MoS₂, can eliminate surface ligand interactions with the rest of the device, however the ligand can still interact at the BN interface causing issues with electron transport [203–205]. Implementing 2D AIP NCs, such as CsPbBr₃ NSs, with increased charge transfer layers like carbon based films or carbon nanotubes can improve

responsivity and therefore photodetector performance to superseded issues with charge carrier mobility [204,205]. For example, the ultrahigh performance of graphene/CsPbBr_{3-x}I_x NC hybrid phototransistors was mainly attributed to the hole transfer from the CsPbBr_{3-x}I_x NCs to graphene and therefore, the high carrier mobility of graphene. However, this photodetector showed a long rise or decay time of 0.81 or 3.65 s, because the charge transport was slowed down by the long-chain organic ligands of CsPbBr_{3-x}I_x NCs [206]. While heterojunction nanocomposites are excellent approaches for resolving surface interaction interference, and improving charge transport and stability. Additionally, ligands still exist at the interface between the perovskite and graphene causing charge transport interference.

The use of surface doped 2D AIP NCs to both improve charge transport and suppress ligand interfacial interactions would be a more widely applicable and industrially relevant approach to improving surface interactions. Xie et al.'s has shown to produce 2D NCs by utilizing Sn⁴⁺ to interact with surface ligand [119,146]. Therefore, it is likely that surface doping through a similar approach would reduce surface ligand interactions, while also providing conductive surface materials to improve charge transport. Alternatively, the unorthodox approach of utilizing doped nanocomposites offers an interesting substitute for the aforementioned heterostructured devices. A recent report by Zheng et al. showed that Mn:CdS/ZnS NCs encapsulated by SiO₂ and surface decorated with Pt NCs could produce catalytic properties due to the long lifetime of Mn²⁺ doped in the CdS core [175]. Utilizing a similar method with 2D AIP NCs, would provide a protective surface, while increasing charge transport. This approach primarily works due to an energy transfer pathway that separates the charge carriers for improved catalytic response [175].

6. Conclusions and perspectives

In conclusion, the discrete manipulation of A, B and X-sites of ABX₃ perovskite structures has proven to be an important tool toward improving the stability and applicability of AIP NCs. These materials have the ability to present impressive optical, magnetic, electronic, and structural properties that need to be explored for a wide-array of applications. Current applications heavily utilize the charge transport mobility of 2D AIP NCs by primarily focus on charge transport devices, such as photodetectors. 2D AIP NC application in light emitting devices has been slowed due to the decreased stability of 2D materials. Discrete compositional control should be at the forefront of the future innovation of AIP NCs, with a particular focus on 2D morphologies for their unique properties and simplified applicability. However, there is still a long way to go before these materials are understood or applied nearly as well as 2D hybrid perovskite NCs or 0D AIP NCs. Increased research is needed in 1) elucidating the formation mechanism of 2D AIP perovskite NPLs; 2) the more structurally sound and far less explored 2D lead free AIP NCs; 3) doped 2D AIP NCs with enhanced optical and electric properties; 4) stability of 2D AIP NCs.

1) 2D AIP NC Formation. The formation mechanism of 0D AIP NCs has been carefully studied for a number of years, leading to a general consensus that the NCs form through multiple intermediary steps through a seed mediated approach that occurs within only a few seconds [207–213]. Rogach et al. studied the 0D NC formation mechanism by a slowed down microwave assisted approach where the CsCO₃ and PbBr₂ precursor powders were separated to opposing sides of a microwave reaction vessel [211]. The solvents and ligands (ODE, OA, and OAm) were carefully added to ensure the powders would not mix yet covered both powders making a filled reaction vessel. This process slowed the normal for-

mation of the as synthesized CsPbBr₃ NCs from a few seconds to nearly 25 minutes, illustrating that weakly bound bromoplumbate scaffolds formed prior to Cs introduction, which would then be filled from the inside out with Cs [211]. Further contributions from Yu et al. [212] and Bi et al. [213] illuminated the bromoplumbate scaffold as [PbBr₆]⁴⁻ corner-sharing octahedra that formed near instantly upon addition of Br halide into the reaction. Introduction of the Cs-precursor would then fill the interstitial sites during the formation of the CsPbBr₃ NCs.

The formation mechanism behind 2D AIP NCs is much more elusive to date and likely is caused by multiple different processes depending on the reaction conditions. For example, Zheng et al. found that NR formation was likely due to high concentrations of short ligands (OctAm and OctAc) around the rod edges, causing greater packing density and therefore forcing growth in the 1D pattern. Post-synthetic solvothermal treatment of these samples lead to the short ligands on the NR edges to evaporate under the high temperature and pressure allowing form NRs to laterally combine into NPLs, which was further assisted due to the increased pressure of the system [88]. Manna et al. formed similarly quantum confined NPLs utilizing a room temperature mediated approach that followed a very different reaction mechanism, where the NPL thickness was controlled by the amount of HBr added to the system. It was determined that the increased acidic environment caused the OAm capping ligands to protonate, which proceeded to compete with Cs+ ions and slow the NC growth in one-dimension [102]. In fact, Goriely et al. found through both theoretical and experimental results that 2D NC growth is essentially caused by both of these methods, where the key is to incite competitive nucleation of atoms and ligands on crystal facets, causing anisotropic NC formation. Further, he found that using strongly interacting, high boiling point ligands and relatively low temperatures, in comparison to 0D NCs, increases the likelihood of 2D NC formation [214]. There are currently still many unknown variables to make a conclusive verdict on how 2D AIP NPLs form. However, we can illustrate the point that anisotropic growth is produced by propagating competition between binding atoms and the reactive surface environment of the rapidly forming NCs. Further investigations are still needed for a more conclusive mechanism.

2) 2D lead free AIP NCs. Current efforts have led to the development of multiple lead free systems [215-218], however, much effort is still needed to make them properly applicable in real world environments. Expanding current research efforts in more structurally sound 2D AIP NCs, especially lead-free alternatives based on Sn, Sb, Ge, Bi, etc. is highly needed. Structural manipulation has been one prevailing factor that has led to many lead-free double-perovskite (A2B2X6) and RP NCs as environmentally friendly alternatives to lead-based AIP NCs. In double-perovskites the Bsite is replaced by M3+ and M+ ions following the morphology A2BB'X6, while RP NCs, layered perovskites with A2BX4 crystal structure, follow a similar structural scheme to ABX₃ NCs. Significant effort has been made to improve these structures by doping [219-222] and morphological control [222–224] to improve the NCs efficiency, PL OY, and stability. For example, RP NCs have shown a keen ability for direct formation of extremely thin 2D NCs that intrinsically prefer a layer 2D morpholgy [225,226]. Despite being promising materials, current research indicates that doubleperovskites have significantly lower PL QYs and comparable

- stabilities to current AIP NCs [227–229]. Therefore, more effort is needed to embolden future applications of these 2D materials.
- 3) Doped 2D AIP NCs with enhanced optical and electric properties. Pradhan et al.'s [74] recent report detailing the doping of Mn²⁺ into 2D Cs₂PbCl₂I₂ NPLs with interesting host-todopant and host bandgap relaxation charge transfer properties that result in an increase in PL response at low temperatures [74]. Similarly, increased PL QY and lifetime decay dynamics have been reported in doped chalcogenide NCs [230–232], however multiple reports on Mn²⁺-doped CsPbCl₃, and CsPbCl_{3-x}Br_x NCs have rather shown a decreased PL response at decreased temperatures [233-236]. At this point, the thermodynamic behavior of dopants in perovskite systems is still unclear, and therefore warrants further study to elucidate the true electron dynamics for a general family of perovskite NCs, including 2D AIP NCs. Additionally, there are still a slew of new dopants that have been explored in lower dimensional perovskite NCs, that yet still need to be explored in 2D AIP NCs, including many other transition metal ions (Ag⁺, Co²⁺, Cu²⁺, Ni²⁺, et al.) [219,237–241], rare-earth metal ions (Ce³⁺, Dy³⁺, Er³⁺, Eu³⁺, Yb³⁺, et al.) [113,242-246], as well as alkaline and alkaline-earth metal ions. These doped OD NCs have shown impressive properties especially for optoelectronic applications. One of the key interests in these doped materials is the fabrication of single component white light emitting sources capable for applications as white-light emitting diodes (LEDs) and lasers [117,118]. Further exploration of dual doping by introducing two different types of dopant ions in perovskites becomes the next clear objective to further increase the NC luminescent response, with a few examples already present in the literature [247-249]. Co-doped AIP NPLs could be created using a combination of a CsPbCl₃ host doped with Mn²⁺ as an orange-red emissive dopant and Er³⁺ as a green/yellow emissive dopant for a near perfect white light emitter given the proper host and dopant intensities. Additionally, dual lanthanide dopants, such as Er³⁺ and Yb³⁺, could be used in a similar system to provide a strong green and NIR red emission, respectively, as lanthanides have shown capable of producing massive increases in PL QY.
- 4) Stability of 2D AIP NCs. Stability is even more of an issue with 2D AIP NCs, as thinner NCs have a larger and more reactive surface area, causing quicker degradation in the presence of oxygen, moisture, and light irradiation, which can be easily demonstrated by exposing 2D perovskite NCs to the electron beam of a transmission electron microscope. Even short exposure times can lead to thin 2D NC melting and degradation, causing the formation of lead clusters within the NC. To overcome these obstacles, more synthetic versatility must be utilized to improve environmental, phase, and morphological stability. For example, a recent publication showed that the incorporation of 23.13% Mg² into B-site of OD CsPbBr3 NCs significantly improved both the PL QY, from 51 to ~100%, and the NCs stability in ambient conditions, under UV-light irradiation, and in polar solvent [250]. The increased stability of the doped NCs can be understood by the increased Goldschmidt tolerance factor. as t is increased from 0.907 to 0.926 by replacing ~23.4% Pb²⁺ with the smaller Mg²⁺ ions. It should be noted that the Goldschmidt tolerance factor does not, however, provide methods of estimating stability based on surface chemistry, size, or shape, nor does it account for the ionic nature of perovskites, which makes them highly structurally and chemi-

cally unstable in conditions containing oxygen, moisture, heat, and continuous illumination; all conditions necessary for many real-world applications [21,158,162].

Consequently, with proper treatment of all three (A, B, and X) ion sites, in 2D ABX₃ AIP NCs, largely variable environmentally friendly products are possible, with improved stability and functionality. Further efforts will be needed to improve 2D AIP stability in environmental conditions while also maintaining their optically active phase and the resulting electric properties. We envision that the future development of these functional 2D AIP NCs with wide lateral dimensions and controlled discrete thicknesses will lead to the development of an improved fundamental understanding of the 2D quantum confined systems as well as the next generation energy harvesting materials for optoelectronic applications.

Declaration of Competing Interest

The authors declare that they have no known competing financial interests or personal relationships that could have appeared to influence the work reported in this paper.

Acknowledgments

W.Z. acknowledges support from Syracuse University under the Collaboration for Unprecedented Success and Excellence (CUSE) Grant (SD-10-2020), ACS Petroleum Research Fund under Award Number 59861-DNI5, and NSF CAREER under Award Number CHE-1944978.

References

- [1] J. Burschka, N. Pellet, S.J. Moon, R. Humphry-Baker, P. Gao, M.K. Nazeeruddin, M. Gratzel, Nature 499 (2013) 316-319.
- Q.A. Akkerman, M. Gandini, F. Di Stasio, P. Rastogi, F. Palazon, G. Bertoni, J.M. Ball, M. Prato, A. Petrozza, L. Manna, Nat. Energy 2 (2016) 16194.
- [3] A. Kojima, K. Teshima, Y. Shirai, T. Miyasaka, J. Am. Chem. Soc. 131 (2009) 6050-6051
- [4] S.D. Stranks, H.J. Snaith, Nat. Nanotechnol. 10 (2015) 391-402.
- [5] M.V. Kovalenko, L. Protesescu, M.I. Bodnarchuk, Science 358 (2017) 745–750.
- [6] Q.A. Akkerman, G. Raino, M.V. Kovalenko, L. Manna, Nat. Mater. 17 (2018)
- [7] F. Meinardi, Q.A. Akkerman, F. Bruni, S. Park, M. Mauri, Z. Dang, L. Manna, S. Brovelli, ACS Energy Lett. 2 (2017) 2368-2377.
- A. Swarnkar, A.R. Marshall, E.M. Sanehira, B.D. Chernomordik, D.T. Moore, J.A. Christians, T. Chakrabarti, J.M. Luther, Science 354 (2016) 92-95.
- G.H. Ahmed, J. Yin, O.M. Bakr, O.F. Mohammed, J. Chem. Phys. 152 (2020) 020902
- [10] I. Dursun, C. Shen, M.R. Parida, J. Pan, S.P. Sarmah, D. Priante, N. Alyami, J. Liu, M.I. Saidaminov, M.S. Alias, A.L. Abdelhady, T.K. Ng, O.F. Mohammed, B.S. Ooi, O.M. Bakr, ACS Photon. 3 (2016) 1150-1156.
- Y. Wang, L. Song, Y. Chen, W. Huang, ACS Photon. 7 (2020) 10-28.
- [12] H. Zhu, Y. Fu, F. Meng, X. Wu, Z. Gong, Q. Ding, M.V. Gustafsson, M.T. Trinh, S. Jin, X.Y. Zhu, Nat. Mater. 14 (2015) 636-642.
- [13] Y. Wang, X.M. Li, V. Nalla, H.B. Zeng, H.D. Sun, Adv. Funct. Mater. 27 (2017) 1605088.
- [14] A. Waleed, M.M. Tavakoli, L. Gu, S. Hussain, D. Zhang, S. Poddar, Z. Wang, R. Zhang, Z. Fan, Nano Lett. 17 (2017) 4951-4957.
- [15] J.N. Chen, Y.M. Shi, Y.B. He, T.Y. Zhai, Flatchem. 17 (2019) 100116.
- Q. Wang, S. Yu, W. Qin, X. Wu, Nanoscale Adv. 2 (2020) 274-285.
- [17] L.Y. Wu, Y.F. Mu, X.X. Guo, W. Zhang, Z.M. Zhang, M. Zhang, T.B. Lu, Angew. Chem. Int. Ed. Engl. 58 (2019) 9491–9495.
- [18] B. Wang, J. Iocozzia, M. Zhang, M. Ye, S. Yan, H. Jin, S. Wang, Z. Zou, Z. Lin, Chem. Soc. Rev. 48 (2019) 4854-4891.
- [19] X. Liu, D. Yu, X. Song, H. Zeng, Small 14 (2018) e1801460.
 [20] M. Saliba, T. Matsui, J.Y. Seo, K. Domanski, J.P. Correa-Baena, M.K. Nazeeruddin, S.M. Zakeeruddin, W. Tress, A. Abate, A. Hagfeldt, M. Gratzel, Energy Environ. Sci. 9 (2016) 1989-1997.
- [21] J. Shamsi, A.S. Urban, M. Imran, L. De Trizio, L. Manna, Chem. Rev. 119 (2019)
- [22] X. He, Y. Qiu, S. Yang, Adv. Mater. 29 (2017) 1700775.
- [23] Y. Zhao, K. Zhu, Chem. Soc. Rev. 45 (2016) 655-689.
- [24] S.D. Stranks, G.E. Eperon, G. Grancini, C. Menelaou, M.J.P. Alcocer, T. Leijtens, L.M. Herz, A. Petrozza, H.J. Snaith, Science 342 (2013) 341-344.
- [25] Y. Yamada, T. Nakamura, M. Endo, A. Wakamiya, Y. Kanemitsu, J. Am. Chem. Soc. 136 (2014) 11610-11613.

- [26] M. Saba, M. Cadelano, D. Marongiu, F. Chen, V. Sarritzu, N. Sestu, C. Figus, M. Aresti, R. Piras, A.G. Lehmann, C. Cannas, A. Musinu, F. Quochi, A. Mura, G. Bongiovanni, Nat. Commun. 5 (2014) 5049.
- [27] D.A. Egger, A.M. Rappe, L. Kronik, Acc. Chem. Res. 49 (2016) 573-581.
- [28] D. Aldakov, P. Reiss, J. Phys. Chem. C 123 (2019) 12527–12541.
- [29] L.C. Schmidt, A. Pertegas, S. Gonzalez-Carrero, O. Malinkiewicz, S. Agouram, G. Minguez Espallargas, H.J. Bolink, R.E. Galian, J. Perez-Prieto, J. Am. Chem. Soc. 136 (2014) 850-853.
- [30] F. Zhang, H. Zhong, C. Chen, X.G. Wu, X. Hu, H. Huang, J. Han, B. Zou, Y. Dong, ACS Nano 9 (2015) 4533-4542.
- [31] Y.X. Li, X.Y. Zhang, H. Huang, S.V. Kershaw, A.L. Rogach, Mater. Today 32 (2020) 204-221.
- [32] D. Weber, znb. 33 (1978) 1443-1445.
- [33] J. Li, C.C. Stoumpos, G.G. Trimarchi, I. Chung, L. Mao, M. Chen, M.R. Wasielewski, L. Wang, M.G. Kanatzidis, Chem. Mater. 30 (2018) 4847–4856.
- [34] M.B. Faheem, B. Khan, C. Feng, M.U. Farooq, F. Raziq, Y. Xiao, Y. Li, ACS Energy Lett. 5 (2019) 290-320.
- [35] M. Kulbak, S. Gupta, N. Kedem, I. Levine, T. Bendikov, G. Hodes, D. Cahen, J. Phys. Chem. Lett. 7 (2016) 167-172.
- [36] J. Li, L. Xu, T. Wang, J. Song, J. Chen, J. Xue, Y. Dong, B. Cai, Q. Shan, B. Han, H. Zeng, Adv. Mater. 29 (2017) 1603885.
- [37] A.B. Wong, Y. Bekenstein, J. Kang, C.S. Kley, D. Kim, N.A. Gibson, D. Zhang, Y. Yu, S.R. Leone, L.W. Wang, A.P. Alivisatos, P. Yang, Nano Lett. 18 (2018) 2060-
- [38] N. Kedem, T.M. Brenner, M. Kulbak, N. Schaefer, S. Levcenko, I. Levine, D. Abou-Ras, G. Hodes, D. Cahen, J. Phys. Chem. Lett. 6 (2015) 2469–2476.
- [39] M.H. Kumar, S. Dharani, W.L. Leong, P.P. Boix, R.R. Prabhakar, T. Baikie, C. Shi, H. Ding, R. Ramesh, M. Asta, M. Graetzel, S.G. Mhaisalkar, N. Mathews, Adv. Mater. 26 (2014) 7122-7127.
- [40] J.H. Im, I.H. Jang, N. Pellet, M. Gratzel, N.G. Park, Nat. Nanotechnol. 9 (2014) 927-932.
- [41] P. Tyagi, S.M. Arveson, W.A. Tisdale, J. Phys. Chem. Lett. 6 (2015) 1911-1916.
- [42] Q.A. Akkerman, V. D'Innocenzo, S. Accornero, A. Scarpellini, A. Petrozza, M. Prato, L. Manna, J. Am. Chem. Soc. 137 (2015) 10276–10281.
- [43] V.A. Hintermayr, A.F. Richter, F. Ehrat, M. Doblinger, W. Vanderlinden, J.A. Sichert, Y. Tong, L. Polavarapu, J. Feldmann, A.S. Urban, Adv. Mater. 28 (2016)
- [44] Q. Wang, X.D. Liu, Y.H. Qiu, K. Chen, L. Zhou, Q.Q. Wang, AIP Adv. 8 (2018) 025108.
- [45] D.P. McMeekin, G. Sadoughi, W. Rehman, G.E. Eperon, M. Saliba, M.T. Horantner, A. Haghighirad, N. Sakai, L. Korte, B. Rech, M.B. Johnston, L.M. Herz, H.J. Snaith, Science 351 (2016) 151-155.
- [46] D.M. Jang, K. Park, D.H. Kim, J. Park, F. Shojaei, H.S. Kang, J.P. Ahn, J.W. Lee, J.K. Song, Nano Lett. 15 (2015) 5191-5199.
- [47] A. Mancini, P. Quadrelli, C. Milanese, M. Patrini, G. Guizzetti, L. Malavasi, Inorg. Chem. 54 (2015) 8893-8895.
- [48] J.B. Hoffman, A.L. Schleper, P.V. Kamat, J. Am. Chem. Soc. 138 (2016) 8603-8611
- [49] B.B. Luo, F. Li, K. Xu, Y. Guo, Y. Liu, Z.G. Xia, J.Z. Zhang, J. Mater. Chem. C 7 (2019) 2781-2808. [50] A.K. Guria, S.K. Dutta, S. Das Adhikari, N. Pradhan, ACS Energy Lett. 2 (2017)
- 1014-1021. [51] K.Z. Du, X.M. Wang, Q.W. Han, Y.F. Yan, D.B. Mitzi, ACS Energy Lett. 2 (2017)
- 2486-2490. [52] J. Zhang, X. Gan, H. Sun, H. Yuan, L. Yu, Z. Hu, Y. Zhu, Sol. RRL 4 (2019)
- 1900227. [53] Z. Yao, Z.W. Jin, X.R. Zhang, Q. Wang, H. Zhang, Z. Xu, L.M. Ding, S.Z. Liu, J.
- Mater. Chem. C 7 (2019) 13736-13742. [54] R. Begum, M.R. Parida, A.L. Abdelhady, B. Murali, N.M. Alyami, G.H. Ahmed, M. N. Hedhili, O.M. Bakr, O.F. Mohammed, J. Am. Chem. Soc. 139 (2017) 731-
- [55] A. Swarnkar, V.K. Ravi, A. Nag, ACS Energy Lett. 2 (2017) 1089-1098.
- [56] W. Liu, Q. Lin, H. Li, K. Wu, I. Robel, J.M. Pietryga, V.I. Klimov, J. Am. Chem. Soc. 138 (2016) 14954-14961.
- [57] Q.A. Akkerman, D. Meggiolaro, Z. Dang, F. De Angelis, L. Manna, ACS Energy Lett. 2 (2017) 2183-2186.
- [58] A. Swarnkar, W.J. Mir, A. Nag, ACS Energy Lett. 3 (2018) 286-289.
- [59] S.K. Dutta, A. Dutta, S. Das Adhikari, N. Pradhan, ACS Energy Lett. 4 (2018) 343-351
- [60] Q. Wang, X.S. Zhang, Z.W. Jin, J.R. Zhang, Z.F. Gao, Y.F. Li, S.Z.F. Liu, ACS Energy Lett. 2 (2017) 1479-1486.
- [61] J.S. Yao, J. Ge, B.N. Han, K.H. Wang, H.B. Yao, H.L. Yu, J.H. Li, B.S. Zhu, J.Z. Song, C. Chen, Q. Zhang, H.B. Zeng, Y. Luo, S.H. Yu, J. Am. Chem. Soc. 140 (2018) 3626-3634.
- [62] W. van der Stam, J.J. Geuchies, T. Altantzis, K.H. van den Bos, J.D. Meeldijk, S. Van Aert, S. Bals, D. Vanmaekelbergh, C. de Mello Donega, J. Am. Chem. Soc. 139 (2017) 4087-4097.
- [63] S. Zou, Y. Liu, J. Li, C. Liu, R. Feng, F. Jiang, Y. Li, J. Song, H. Zeng, M. Hong, X. Chen, J. Am. Chem. Soc. 139 (2017) 11443-11450.
- [64] H. Liu, Z. Wu, J. Shao, D. Yao, H. Gao, Y. Liu, W. Yu, H. Zhang, B. Yang, ACS Nano 11 (2017) 2239-2247.
- [65] D.M. Trots, S.V. Myagkota, J. Phys. Chem. Solids 69 (2008) 2520-2526.
- [66] P. Todorović, D. Ma, B. Chen, R. Quintero-Bermudez, M.I. Saidaminov, Y. Dong, Z.H. Lu, E.H. Sargent, Adv. Opt. Mater. 7 (2019) 1901440.
- Z.J. Li, E. Hofman, A.H. Davis, A. Khammang, J.T. Wright, B. Dzikovski, R.W. Meulenberg, W.W. Zheng, Chem. Mater. 30 (2018) 6400-6409.

- [68] W.J. Mir, M. Jagadeeswararao, S. Das, A. Nag, ACS Energy Lett. 2 (2017) 537-
- [69] S. Das Adhikari, A. Dutta, S.K. Dutta, N. Pradhan, ACS Energy Lett. 3 (2018) 1247-1253.
- [70] C. Liu, J. Lin, W. Zhai, Z.K. Wen, X. He, M.M. Yu, Y. Huang, Z.L. Guo, C. Yu, C.C. Tang, RSC Adv. 9 (2019) 39315-39322.
- [71] T.C. He, J.Z. Li, X. Qiu, S.Y. Xiao, X.D. Lin, Photon. Res. 6 (2018) 1021–1027.
- 72] D. Parobek, Y.T. Dong, T. Qiao, D.H. Son, Chem. Mater. 30 (2018) 2939-2944.
- [73] W.J. Mir, Y. Mahor, A. Lohar, M. Jagadeeswararao, S. Das, S. Mahamuni, A. Nag, Chem. Mater. 30 (2018) 8170-8178.
- [74] A. Dutta, R.K. Behera, S. Deb, S. Baitalik, N. Pradhan, J. Phys. Chem. Lett. 10 (2019) 1954-1959.
- R. Ketavath, N.K. Katturi, S.G. Ghugal, H.K. Kolli, T. Swetha, V.R. Soma, B. Murali, J. Phys. Chem. Lett. 10 (2019) 5577-5584.
- [76] H. Zhang, Z.H. Zhan, C. Ma, Y.Q. Liu, H.P. Xie, S.Q. Luo, Y.B. Yuan, Y.L. Gao, Y. Zhang, W.Q. Ming, Y. Liu, A.L. Pan, B. Yang, J. Mater. Chem. C 7 (2019) 5488-
- [77] S. Bera, D. Ghosh, A. Dutta, S. Bhattacharyya, S. Chakraborty, N. Pradhan, ACS Energy Lett. 4 (2019) 1364-1369.
- X. Zhang, H. Liu, W. Wang, J. Zhang, B. Xu, K.L. Karen, Y. Zheng, S. Liu, S. Chen, K. Wang, X.W. Sun, Adv. Mater. 29 (2017) 1606405.
- [79] X. Zhang, W. Wang, B. Xu, H. Liu, H. Shi, H. Dai, X. Zhang, S. Chen, K. Wang, X. W. Sun, ACS Appl. Mater. Interfaces 10 (2018) 24242-24248.
- [80] I. Lignos, V. Morad, Y. Shynkarenko, C. Bernasconi, R.M. Maceiczyk, L. Protesescu, F. Bertolotti, S. Kumar, S.T. Ochsenbein, N. Masciocchi, A. Guagliardi, C.J. Shih, M.I. Bodnarchuk, A.J. deMello, M.V. Kovalenko, ACS Nano 12 (2018) 5504-5517.
- [81] B. Xu, W.G. Wang, X.L. Zhang, W.Y. Cao, D. Wu, S. Liu, H.T. Dai, S.M. Chen, K. Wang, X.W. Sun, J. Mater. Chem. C 5 (2017) 6123-6128.
- [82] J.J. Gallardo, E. Blanco, A. Sanchez-Coronilla, J.C. Pinero, J. Navas, Appl. Mater. Today 18 (2020) 100488.
- [83] X. Meng, Z. Wang, W. Qian, Z. Zhu, T. Zhang, Y. Bai, C. Hu, S. Xiao, Y. Yang, S. Yang, J. Phys. Chem. Lett. 10 (2019) 194–199.
- [84] Y. Guo, F. Zhao, Z. Li, J. Tao, D. Zheng, J. Jiang, J. Chu, Org. Electron. 83 (2020)
- [85] D. Bai, J. Zhang, Z. Jin, H. Bian, K. Wang, H. Wang, L. Liang, Q. Wang, S.F. Liu, ACS Energy Lett. 3 (2018) 970-978.
- [86] U. Khan, Y. Zhinong, A.A. Khan, A. Zulfiqar, N. Ullah, Nanoscale Res. Lett. 14
- [87] C.F.J. Lau, M. Zhang, X.F. Deng, J.H. Zheng, J.M. Bing, Q.S. Ma, J. Kim, L. Hu, M.A. Green, S.J. Huang, A. Ho-Baillie, ACS Energy Lett. 2 (2017) 2319-2325.
- [88] Z.-J. Li, E. Hofman, A.H. Davis, M.M. Maye, W. Zheng, Chem. Mater. 30 (2018) 3854-3860.
- [89] A.M. Elseman, M.M. Rashad, A.M. Hassan, ACS Sustain. Chem. Eng. 4 (2016) 4875-4886.
- [90] J. Zhang, X. Yang, H. Deng, K. Qiao, U. Farooq, M. Ishaq, F. Yi, H. Liu, J. Tang, H. Song, Nanomicro Lett. 9 (2017) 36.
- [91] L. Martinez-Sarti, S.H. Jo, Y.H. Kim, M. Sessolo, F. Palazon, T.W. Lee, H.J. Bolink, Nanoscale 11 (2019) 12793-12797.
- [92] C. Zhou, Y. Tian, M. Wang, A. Rose, T. Besara, N.K. Doyle, Z. Yuan, J.C. Wang, R. Clark, Y. Hu, T. Siegrist, S. Lin, B. Ma, Angew. Chem. Int. Ed. Engl. 56 (2017) 9018-9022.
- [93] S.W. Eaton, M. Lai, N.A. Gibson, A.B. Wong, L. Dou, J. Ma, L.W. Wang, S.R. Leone, P. Yang, Proc. Natl. Acad. Sci. U.S.A. 113 (2016) 1993-1998.
- [94] B.J. Bohn, Y. Tong, M. Gramlich, M.L. Lai, M. Doblinger, K. Wang, R.L.Z. Hoye, P. Muller-Buschbaum, S.D. Stranks, A.S. Urban, L. Polavarapu, J. Feldmann, Nano Lett. 18 (2018) 5231-5238.
- [95] M.C. Weidman, A.J. Goodman, W.A. Tisdale, Chem. Mater. 29 (2017) 5019-5030
- [96] M.L. De Giorgi, A. Perulli, N. Yantara, P.P. Boix, M. Anni, J. Phys. Chem. C. 121 (2017) 14772–14778.
- [97] D. Chen, X. Chen, J. Li, X. Li, J. Zhong, Dalton Trans. 47 (2018) 9845–9849.[98] S. Chen, G. Shi, Adv. Mater. 29 (2017) 1605448.
- Y. Bekenstein, B.A. Koscher, S.W. Eaton, P. Yang, A.P. Alivisatos, J. Am. Chem. [99] Soc. 137 (2015) 16008-16011.
- [100] C. Tan, X. Cao, X.J. Wu, Q. He, J. Yang, X. Zhang, J. Chen, W. Zhao, S. Han, G.H. Nam, M. Sindoro, H. Zhang, Chem. Rev. 117 (2017) 6225–6331. [101] F. Bertolotti, G. Nedelcu, A. Vivani, A. Cervellino, N. Masciocchi, A. Guagliardi,
- M.V. Kovalenko, ACS Nano 13 (2019) 14294-14307.
- [102] Q.A. Akkerman, S.G. Motti, A.R. Srimath Kandada, E. Mosconi, V. D'Innocenzo, G. Bertoni, S. Marras, B.A. Kamino, L. Miranda, F. De Angelis, A. Petrozza, M.
- Prato, L. Manna, J. Am. Chem. Soc. 138 (2016) 1010–1016. [103] J. Yu, J. Kong, W. Hao, X. Guo, H. He, W.R. Leow, Z. Liu, P. Cai, G. Qian, S. Li, X. Chen, X. Chen, Adv. Mater. 31 (2019) e1806385.
- [104] A. Biswas, R. Bakthavatsalam, J. Kundu, Chem. Mater. 29 (2017) 7816-7825.
- [105] C. Sun, Z. Gao, Y. Deng, H. Liu, L. Wang, S. Su, P. Li, H. Li, Z. Zhang, W. Bi, ACS Appl. Mater. Interfaces 11 (2019) 34109–34116.
- [106] J.P. Correa-Baena, Y. Luo, T.M. Brenner, J. Snaider, S. Sun, X. Li, M.A. Jensen, N. T.P. Hartono, L. Nienhaus, S. Wieghold, J.R. Poindexter, S. Wang, Y.S. Meng, T. Wang, B. Lai, M.V. Holt, Z. Cai, M.G. Bawendi, L. Huang, T. Buonassisi, D.P. Fenning, Science 363 (2019) 627-631.
- [107] T. Li, X. Chen, X. Wang, H. Lu, Y. Yan, M.C. Beard, D.B. Mitzi, ACS Energy Lett. 5 (2019) 347-352.
- [108] L. Dou, A.B. Wong, Y. Yu, M. Lai, N. Kornienko, S.W. Eaton, A. Fu, C.G. Bischak, J. Ma, T. Ding, N.S. Ginsberg, L.W. Wang, A.P. Alivisatos, P. Yang, Science 349 (2015) 1518-1521.

- [109] Y. Zhou, J. Chen, O.M. Bakr, H.T. Sun, Chem. Mater. 30 (2018) 6589-6613.
- [110] N. Phung, R. Felix, D. Meggiolaro, A. Al-Ashouri, E.S.G. Sousa, C. Hartmann, J. Hidalgo, H. Kobler, E. Mosconi, B. Lai, R. Gunder, M. Li, K.L. Wang, Z.K. Wang, K. Nie, E. Handick, R.G. Wilks, J.A. Marquez, B. Rech, T. Unold, J.P. Correa-Baena, S. Albrecht, F. De Angelis, M. Bar, A. Abate, J. Am. Chem. Soc. 142 (2020) 2364-2374.
- [111] L. Xu, S. Yuan, H. Zeng, J. Song, Mater. Today Nano 6 (2019) 100036.
- [112] X. Zhang, L. Li, Z. Sun, J. Luo, Chem. Soc. Rev. 48 (2019) 517-539.
- [113] W.J. Mir, T. Sheikh, H. Arfin, Z.G. Xia, A. Nag, Npg Asia Mater. 12 (2020) 9.
- [114] R. Rajeswari, N. Islavath, M. Raghavender, L. Giribabu, Chem. Rec. 20 (2020) 65-88
- [115] A.R. Kirmani, A.E. Mansour, C. Yang, R. Munir, A.M. El-Zohry, O.F. Mohammed, A. Amassian, PLoS One 15 (2020) e0230540.
- [116] G.C. Adhikari, S. Thapa, H.Y. Zhu, P.F. Zhu, Adv. Opt. Mater. 7 (2019) 1900916.
- [117] H. Wu, S. Xu, H. Shao, L. Li, Y. Cui, C. Wang, Nanoscale 9 (2017) 16858-16863.
- [118] F. Jiang, W. Zheng, Y. Jiang, Y. Li, P. Fan, W. Huang, X. Fu, L. Li, Y. Ouyang, X. Zhu, X. Zhuang, A. Pan, J. Phys. Chem. Lett. 11 (2020) 3320-3326.
- [119] X. Dong, E. Acheampong Tsiwah, T. Li, J. Hu, Z. Li, Y. Ding, Z. Deng, W. Chen, L. Xu, P. Gao, X. Zhao, Y. Xie, Nanoscale 11 (2019) 7903-7912.
- [120] S. Thapa, G.C. Adhikari, H.Y. Zhu, P.F. Zhu, J. Opt. Soc. Am. B 36 (2019) 1616-1622.
- [121] D.J. Yu, B. Cai, F. Cao, X.M. Li, X.H. Liu, Y. Zhu, J.P. Ji, Y. Gu, H.B. Zeng, Adv. Mater. Interfaces 4 (2017) 1700441.
- [122] E.A. Tsiwah, Y.X. Ding, Z.X. Li, Z.Y. Zhao, M.Q. Wang, C. Hu, X.Q. Liu, C.H. Sun, X.J. Zhao, Y. Xie, Crysteng. Comm. 19 (2017) 7041-7049.
- [123] C.H. Li, C.C. Tsai, M.Y. Liao, Y.A. Su, S.T. Lin, C.C. Chueh, Nanoscale 11 (2019) 2608-2616.
- [124] Y. Numata, Y. Sanehira, R. Ishikawa, H. Shirai, T. Miyasaka, ACS Appl. Mater. Interfaces 10 (2018) 42363-42371.
- [125] N.G. Park, Mater. Today 18 (2015) 65-72.
- [126] P. Reiss, M. Carriere, C. Lincheneau, L. Vaure, S. Tamang, Chem. Rev. 116 (2016) 10731-10819.
- [127] B.A. Rosales, M.P. Hanrahan, B.W. Boote, A.J. Rossini, E.A. Smith, J. Vela, ACS Energy Lett. 2 (2017) 906-914.
- [128] E. Shi, Y. Gao, B.P. Finkenauer, Akriti, A.H. Coffey, L. Dou, Chem. Soc. Rev. 47 (2018) 6046-6072.
- [129] Q. Zhang, Y. Yin, A.C.S. Cent, Sci. 4 (2018) 668-679.
- [130] Z.-J. Li, E. Hofman, J. Li, A.H. Davis, C.-H. Tung, L.-Z. Wu, W. Zheng, Adv. Funct. Mater. 28 (2018) 1704288.
- [131] X. Li, F. Cao, D. Yu, J. Chen, Z. Sun, Y. Shen, Y. Zhu, L. Wang, Y. Wei, Y. Wu, H. Zeng, Small 13 (2017) 1603996.
- [132] A. Pan, B. He, X. Fan, Z. Liu, J.J. Urban, A.P. Alivisatos, L. He, Y. Liu, ACS Nano 10 (2016) 7943-7954.
- [133] D. Yu, C. Yin, F. Cao, Y. Zhu, J. Ji, B. Cai, X. Liu, X. Wang, H. Zeng, ACS Appl. Mater. Interfaces 9 (2017) 39602–39609.
- [134] H. Hu, Z. Han, B. Huang, Y. Dong, Y. Zou, J. Colloid. Inter. Sci. 554 (2019) 619-626
- [135] S. Sun, D. Yuan, Y. Xu, A. Wang, Z. Deng, ACS Nano 10 (2016) 3648-3657.
- [136] B. Luo, Y.C. Pu, S.A. Lindley, Y. Yang, L. Lu, Y. Li, X. Li, J.Z. Zhang, Angew. Chem. Int. Ed. Engl. 55 (2016) 8864-8868.
- [137] S. Yun, A. Kirakosyan, S.G. Yoon, J. Choi, ACS Sustain. Chem. Eng. 6 (2018) 3733-3738.
- [138] H. Huang, Y. Li, Y. Tong, E.P. Yao, M.W. Feil, A.F. Richter, M. Doblinger, A.L. Rogach, J. Feldmann, L. Polavarapu, Angew. Chem. Int. Ed. Engl. 58 (2019) 16558-16562.
- [139] Z. Dang, B. Dhanabalan, A. Castelli, R. Dhall, K.C. Bustillo, D. Marchelli, D. Spirito, U. Petralanda, J. Shamsi, L. Manna, R. Krahne, M.P. Arciniegas, Nano Lett. 20 (2020) 1808-1818.
- [140] H. Huang, Q. Xue, B. Chen, Y. Xiong, J. Schneider, C. Zhi, H. Zhong, A.L. Rogach, Angew. Chem. Int. Ed. Engl. 56 (2017) 9571–9576.

 [141] D. Zhang, S.W. Eaton, Y. Yu, L. Dou, P. Yang, J. Am. Chem. Soc. 137 (2015)
- 9230-9233
- [142] Q. Pan, H. Hu, Y. Zou, M. Chen, L. Wu, D. Yang, X. Yuan, J. Fan, B. Sun, Q. Zhang, J. Mater. Chem. C 5 (2017) 10947–10954. [143] J. Shamsi, Z. Dang, P. Bianchini, C. Canale, F.D. Stasio, R. Brescia, M. Prato, L.
- Manna, J. Am. Chem. Soc. 138 (2016) 7240-7243. [144] J.A. Sichert, Y. Tong, N. Mutz, M. Vollmer, S. Fischer, K.Z. Milowska, R. Garcia
- Cortadella, B. Nickel, C. Cardenas-Daw, J.K. Stolarczyk, A.S. Urban, J. Feldmann, Nano Lett. 15 (2015) 6521–6527.
- [145] Z. Yuan, Y. Shu, Y. Tian, Y. Xin, B. Ma, Chem. Commun. 51 (2015) 16385-16388.
- [146] Y.X. Ding, T. Li, X.Y. Li, E.A. Tsiwah, C.Z. Liu, P. Gao, T. Zeng, Y.X. Chen, X.J. Zhao, Y. Xie, Crysteng. Comm. 21 (2019) 2388-2397.
- [147] L. Protesescu, S. Yakunin, M.I. Bodnarchuk, F. Krieg, R. Caputo, C.H. Hendon, R. X. Yang, A. Walsh, M.V. Kovalenko, Nano Lett. 15 (2015) 3692–3696.
- [148] K.-H. Wang, L. Wu, L. Li, H.-B. Yao, H.-S. Qian, S.-H. Yu, Angew. Chem. Int. Ed. 55 (2016) 8328-8332.
- [149] V. Schettino, R. Bini, Chem. Soc. Rev. 36 (2007) 869-880.
- [150] W.W. Zheng, F. Guo, M. Qian, Adv. Funct. Mater. 15 (2005) 331-335.
- [151] H. Fan, Z.H. Wang, X.Z. Liu, W.W. Zheng, F. Guo, Y.T. Qian, Solid State Commun. 135 (2005) 319-322.
- [152] D. Zhang, Y. Yang, Y. Bekenstein, Y. Yu, N.A. Gibson, A.B. Wong, S.W. Eaton, N. Kornienko, Q. Kong, M. Lai, A.P. Alivisatos, S.R. Leone, P. Yang, J. Am. Chem. Soc. 138 (2016) 7236-7239.
- C. Eames, J.M. Frost, P.R. Barnes, B.C. O'Regan, A. Walsh, M.S. Islam, Nat. Commun. 6 (2015) 7497.

- [154] C.C. Lin, K.Y. Xu, D. Wang, A. Meijerink, Sci. Rep. 7 (2017) 45906.[155] G. Nedelcu, L. Protesescu, S. Yakunin, M.I. Bodnarchuk, M.J. Grotevent, M.V. Kovalenko, Nano Lett. 15 (2015) 5635-5640.
- [156] W. Li, Z.M. Wang, F. Deschler, S. Gao, R.H. Friend, A.K. Cheetham, Nat. Rev. Mater. 2 (2017) 16099.
- [157] W. Travis, E.N.K. Glover, H. Bronstein, D.O. Scanlon, R.G. Palgrave, Chem. Sci. 7 (2016) 4548-4556.
- [158] C.J. Bartel, C. Sutton, B.R. Goldsmith, R. Ouyang, C.B. Musgrave, L.M. Ghiringhelli, M. Scheffler, Sci. Adv. 5 (2019) eaav0693.
- [159] J.S. Manser, J.A. Christians, P.V. Kamat, Chem. Rev. 116 (2016) 12956-13008.
- [160] C.C. Stoumpos, M.G. Kanatzidis, Acc. Chem. Res. 48 (2015) 2791–2802.
- [161] M.C. Brennan, J.E. Herr, T.S. Nguyen-Beck, J. Zinna, S. Draguta, S. Rouvimov, J. Parkhill, M. Kuno, J. Am. Chem. Soc. 139 (2017) 12201-12208.
- [162] L. Protesescu, S. Yakunin, S. Kumar, J. Bar, F. Bertolotti, N. Masciocchi, A. Guagliardi, M. Grotevent, I. Shorubalko, M.I. Bodnarchuk, C.J. Shih, M.V. Kovalenko, ACS Nano 11 (2017) 3119-3134.
- [163] D. Chen, X. Chen, Z. Wan, G. Fang, ACS Appl. Mater. Interfaces 9 (2017) 20671-20678.
- [164] A. Hazarika, Q. Zhao, E.A. Gaulding, J.A. Christians, B. Dou, A.R. Marshall, T. Moot, J.J. Berry, J.C. Johnson, J.M. Luther, ACS Nano 12 (2018) 10327-10337.
- [165] C.Y. Wang, Y.K. Zhang, A.F. Wang, Q. Wang, H.Y. Tang, W. Shen, Z. Li, Z.T. Deng, Chem. Mater. 29 (2017) 2157-2166.
- [166] P. Vashishtha, M. Ng, S.B. Shivarudraiah, J.E. Halpert, Chem. Mater. 31 (2019)
- [167] M.P. Hautzinger, D. Pan, A.K. Pigg, Y. Fu, D.J. Morrow, M. Leng, M.-Y. Kuo, N. Spitha, D.P. Lafayette, D.D. Kohler, J.C. Wright, S. Jin, ACS Energy Lett. 5 (2020) 1430-1437.
- [168] J. Li, Q. Yu, Y. He, C.C. Stoumpos, G. Niu, G.G. Trimarchi, H. Guo, G. Dong, D. Wang, L. Wang, M.G. Kanatzidis, J. Am. Chem. Soc. 140 (2018) 11085-11090.
- [169] C.H. Li, M.Y. Liao, C.H. Chen, C.C. Chueh, J. Mater. Chem. C 8 (2020) 4294-
- [170] D. Parobek, B.J. Roman, Y. Dong, H. Jin, E. Lee, M. Sheldon, D.H. Son, Nano Lett. 16 (2016) 7376-7380.
- [171] N. Pradhan, J. Phys. Chem. Lett. 10 (2019) 2574-2577.
- [172] W. Zheng, G.F. Strouse, J. Am. Chem. Soc. 133 (2011) 7482-7489.
- [173] E. Hofman, R.J. Robinson, Z.J. Li, B. Dzikovski, W. Zheng, J. Am. Chem. Soc. 139 (2017) 8878-8885.
- [174] E. Hofman, A. Khammang, J.T. Wright, Z.J. Li, P.F. McLaughlin, A.H. Davis, J.M. Franck, A. Chakraborty, R.W. Meulenberg, W. Zheng, J. Phys. Chem. Lett. 11 (2020) 5992-5999.
- [175] Z.J. Li, S.Y. Li, A.H. Davis, E. Hofman, G. Leem, W.W. Zheng, Nano Res. 13 (2020) 1668-1676.
- [176] A.H. Davis, E. Hofman, K. Chen, Z.J. Li, A. Khammang, H. Zamani, J.M. Franck, M.M. Maye, R.W. Meulenberg, W.W. Zheng, Chem. Mater. 31 (2019) 2516-
- [177] Z.J. Li, E. Hofman, A. Blaker, A.H. Davis, B. Dzikovski, D.K. Ma, W. Zheng, ACS Nano 11 (2017) 12591-12600.
- [178] P. Acharyya, K. Maji, K. Kundu, K. Biswas, ACS Appl. Nano Mater. 3 (2020) 877-886.
- [179] Q.A. Akkerman, E. Bladt, U. Petralanda, Z. Dang, E. Sartori, D. Baranov, A.L. Abdelhady, I. Infante, S. Bals, L. Manna, Chem. Mater. 31 (2019) 2182–2190.
- [180] S. Paul, E. Bladt, A.F. Richter, M. Doblinger, Y. Tong, H. Huang, A. Dey, S. Bals, T. Debnath, L. Polavarapu, J. Feldmann, Angew. Chem. Int. Ed. Engl. 59 (2020) 6794-6799.
- [181] F. Di Stasio, S. Christodoulou, N. Huo, G. Konstantatos, Chem. Mater. 29 2017) 7663-7667.
- [182] J. Pan, Y. Shang, J. Yin, M. De Bastiani, W. Peng, I. Dursun, L. Sinatra, A.M. El-Zohry, M.N. Hedhili, A.-H. Emwas, O.F. Mohammed, Z. Ning, O.M. Bakr, J. Am. Chem. Soc. 140 (2018) 562-565
- [183] G. Li, J. Huang, H. Zhu, Y. Li, J.-X. Tang, Y. Jiang, Chem. Mater. 30 (2018) 6099-6107.
- [184] Y. Gao, L. Zhao, Q. Shang, Y. Zhong, Z. Liu, J. Chen, Z. Zhang, J. Shi, W. Du, Y. Zhang, S. Chen, P. Gao, X. Liu, X. Wang, Q. Zhang, Adv. Mater. 30 (2018) 1801805
- [185] B.D. Folie, J.A. Tan, J. Huang, P.C. Sercel, M. Delor, M. Lai, J.L. Lyons, N. Bernstein, A.L. Efros, P. Yang, N.S. Ginsberg, J. Phys. Chem. A. 124 (2020) 1867-1876
- [186] C.-H. Lin, C.-Y. Kang, T.-Z. Wu, C.-L. Tsai, C.-W. Sher, X. Guan, P.-T. Lee, T. Wu, C.-H. Ho, H.-C. Kuo, J.-H. He, Adv. Funct. Mater. 30 (2020) 1909275.
- [187] Y. Chen, Y. Sun, J. Peng, J. Tang, K. Zheng, Z. Liang, Adv. Mater. 30 (2018) 1703487.
- [188] Z. Li, X. Liu, J. Xu, S. Yang, H. Zhao, H. Huang, S.F. Liu, J. Yao, J. Phys. Chem. Lett. 11 (2020) 4138-4146.
- [189] R.T. Dong, C.Y. Lan, F.Z. Li, S. Yip, J.C. Ho, Nanoscale Horiz. 4 (2019) 1342-1352
- [190] P.H. Wangyang, C.H. Gong, G.F. Rao, K. Hu, X.P. Wang, C.Y. Yan, L.P. Dai, C.Y. Wu, J. Xiong, Adv. Opt. Mater. 6 (2018) 1701302.
- [191] Z. Lai, R. Dong, Q. Zhu, Y. Meng, F. Wang, F. Li, X. Bu, X. Kang, H. Zhang, Q. Quan, W. Wang, F. Wang, S. Yip, J.C. Ho, ACS Appl. Mater. Interfaces (2020).
- [192] A.R.b.M. Yusoff, H.P. Kim, X. Li, J. Kim, J. Jang, M.K. Nazeeruddin, Adv. Mater. 29 (2017) 1602940.
- [193] H. Zhou, J. Zeng, Z. Song, C.R. Grice, C. Chen, Z. Song, D. Zhao, H. Wang, Y. Yan, J. Phys. Chem. Lett. 9 (2018) 2043–2048.
- [194] D. Li, H.-C. Cheng, Y. Wang, Z. Zhao, G. Wang, H. Wu, Q. He, Y. Huang, X. Duan, Adv. Mater. 29 (2017) 1601959.

- [195] D. Li, H.-C. Cheng, H. Wu, Y. Wang, J. Guo, G. Wang, Y. Huang, X. Duan, J. Phys. Chem. Lett. 8 (2017) 429-434.
- [196] D. Li, G. Wang, H.-C. Cheng, C.-Y. Chen, H. Wu, Y. Liu, Y. Huang, X. Duan, Nat. Commun. 7 (2016) 11330.
- [197] J. Song, L. Xu, J. Li, J. Xue, Y. Dong, X. Li, H. Zeng, Adv. Mater. 28 (2016) 4861-4869
- [198] S. Zhou, Y.P. Ma, G.D. Zhou, X. Xu, M.C. Qin, Y.H. Li, Y.J. Hsu, H.L. Hu, G. Li, N. Zhao, J.B. Xu, X.H. Lu, ACS Energy Lett. 4 (2019) 534-541.
- [199] H.-T. Sun, J. Zhou, J. Qiu, Prog. Mater. Sci. 64 (2014) 1-72.
- [200] J. Zaumseil, H. Sirringhaus, Chem. Rev. 107 (2007) 1296-1323.
- [201] X. Liu, D. Yu, F. Cao, X. Li, J. Ji, J. Chen, X. Song, H. Zeng, Small 13 (2017) 1700364.
- [202] C. Huo, X. Liu, Z. Wang, X. Song, H. Zeng, Adv. Opt. Mater. 6 (2018) 1800152.
- [203] H.-C. Cheng, G. Wang, D. Li, Q. He, A. Yin, Y. Liu, H. Wu, M. Ding, Y. Huang, X. Duan, Nano Lett. 16 (2016) 367-373.
- [204] X. Song, X. Liu, D. Yu, C. Huo, J. Ji, X. Li, S. Zhang, Y. Zou, G. Zhu, Y. Wang, M. Wu, A. Xie, H. Zeng, ACS Appl. Mater. Interfaces 10 (2018) 2801-2809.
- [205] X. Li, D. Yu, J. Chen, Y. Wang, F. Cao, Y. Wei, Y. Wu, L. Wang, Y. Zhu, Z. Sun, J. Ji, Y. Shen, H. Sun, H. Zeng, ACS Nano 11 (2017) 2015-2023.
- [206] D.-H. Kwak, D.-H. Lim, H.-S. Ra, P. Ramasamy, J.-S. Lee, RSC Adv. 6 (2016) 65252-65256.
- [207] D.V. Talapin, A.L. Rogach, M. Haase, H. Weller, J. Phys. Chem. B 105 (2001) 12278-12285.
- [208] M. Koolyk, D. Amgar, S. Aharon, L. Etgar, Nanoscale 8 (2016) 6403-6409.
- [209] H. Huang, J. Raith, S.V. Kershaw, S. Kalytchuk, O. Tomanec, L. Jing, A.S. Susha, R. Zboril, A.L. Rogach, Nat. Commun. 8 (2017) 996.
- [210] J. Zhang, L. Fan, J. Li, X. Liu, R. Wang, L. Wang, G. Tu, Nano Res. 12 (2019) 121-
- [211] Y. Li, H. Huang, Y. Xiong, S.V. Kershaw, A.L. Rogach, Angew. Chem. Int. Ed. Engl. 57 (2018) 5833-5837.
- [212] B.-S. Zhu, Z. He, J.-S. Yao, C. Chen, K.-H. Wang, H.-B. Yao, J.-W. Liu, S.-H. Yu, Adv. Opt. Mater. 6 (2018) 1701029.
- [213] C. Sun, Z. Gao, H. Liu, C. Geng, H. Wu, X. Zhang, C. Fan, W. Bi, Dalton Trans. 47 (2018) 16218-16224.
- [214] V.M. Burlakov, Y. Hassan, M. Danaie, H.J. Snaith, A. Goriely, J. Phys. Chem. Lett. 11 (2020) 6535-6543.
- [215] J. Sun, J. Yang, J.I. Lee, J.H. Cho, M.S. Kang, J. Phys. Chem. Lett. 9 (2018) 1573-
- [216] Z. Shi, J. Guo, Y. Chen, Q. Li, Y. Pan, H. Zhang, Y. Xia, W. Huang, Adv. Mater. 29 (2017) 1605005.
- [217] Q. Fan, G.V. Biesold-McGee, J. Ma, Q. Xu, S. Pan, J. Peng, Z. Lin, Angew. Chem. Int. Ed. Engl. 59 (2020) 1030-1046.
- [218] F. Igbari, Z.K. Wang, L.S. Liao, Adv. Energy Mater. 9 (2019) 1803150.
- [219] A. Karmakar, M.S. Dodd, S. Agnihotri, E. Ravera, V.K. Michaelis, Chem. Mater. 30 (2018) 8280-8290.
- [220] Y. Liu, Y.Y. Jing, J. Zhao, Q.L. Liu, Z.G. Xia, Chem. Mater. 31 (2019) 3333–3339.
- [221] Y. Liu, X. Rong, M. Li, M.S. Molokeev, J. Zhao, Z. Xia, Angew. Chem. Int. Ed. Engl. 59 (2020) 11634-11640.
- [222] L. Men, B.A. Rosales, N.E. Gentry, S.D. Cady, J. Vela, ChemNanoMat 5 (2019) 334-339.
- [223] X. Zhang, C. Wang, Y. Zhang, X. Zhang, S. Wang, M. Lu, H. Cui, S.V. Kershaw, W. W. Yu, A.L. Rogach, ACS Energy Lett. 4 (2018) 242-248.
- [224] L.Y. Lian, G.M. Zhai, F. Cheng, Y. Xia, M.Y. Zheng, J.P. Ke, M.Y. Gao, H. Liu, D.L. Zhang, L.Y. Li, J.B. Gao, J. Tang, J.B. Zhang, Crysteng. Comm. 20 (2018) 7473-
- [225] H. Tsai, W. Nie, J.C. Blancon, C.C. Stoumpos, C.M.M. Soe, J. Yoo, J. Crochet, S. Tretiak, J. Even, A. Sadhanala, G. Azzellino, R. Brenes, P.M. Ajayan, V. Bulovic, S.D. Stranks, R.H. Friend, M.G. Kanatzidis, A.D. Mohite, Adv. Mater. 30 (2018) 1704217
- [226] B.V. Beznosikov, K.S. Aleksandrov, Crystallogr. Rep. 45 (2000) 792–798.
 [227] P. Han, X. Mao, S. Yang, F. Zhang, B. Yang, D. Wei, W. Deng, K. Han, Angew. Chem. Int. Ed. Engl. 58 (2019) 17231–17235.
- [228] B. Yang, J. Chen, S. Yang, F. Hong, L. Sun, P. Han, T. Pullerits, W. Deng, K. Han, Angew. Chem. Int. Ed. Engl. 57 (2018) 5359–5363. [229] B. Yang, X. Mao, F. Hong, W. Meng, Y. Tang, X. Xia, S. Yang, W. Deng, K. Han, J.
- Am. Chem. Soc. 140 (2018) 17001–17006.
- [230] V.A. Vlaskin, N. Janssen, J. van Rijssel, R. Beaulac, D.R. Gamelin, Nano Lett. 10 (2010) 3670-3674.
- [231] E.J. McLaurin, L.R. Bradshaw, D.R. Gamelin, Chem. Mater. 25 (2013) 1283-1292.
- [232] R. Beaulac, P.I. Archer, J. van Rijssel, A. Meijerink, D.R. Gamelin, Nano Lett. 8 (2008) 2949-2953.
- [233] X. Yuan, S. Ji, M.C. De Siena, L. Fei, Z. Zhao, Y. Wang, H. Li, J. Zhao, D.R. Gamelin, Chem. Mater. 29 (2017) 8003-8011.
- [234] L. Fei, X. Yuan, J. Hua, M. Ikezawa, R. Zeng, H. Li, Y. Masumoto, J. Zhao, Nanoscale 10 (2018) 19435-19442. [235] W.Z. Wu, W.L. Liu, Q. Wang, Q.J. Han, Q.X. Yang, J. Alloys Compd. 787 (2019)
- 165-172.
- [236] D. Rossi, D. Parobek, Y.T. Dong, D.H. Son, J. Phys. Chem. C 121 (2017) 17143-17149.
- [237] M. Lu, X. Zhang, X. Bai, H. Wu, X. Shen, Y. Zhang, W. Zhang, W. Zheng, H. Song, W.W. Yu, A.L. Rogach, ACS Energy Lett. 3 (2018) 1571-1577.
- [238] Y. Hu, X.Y. Zhang, C.Q. Yang, L. Ji, L. Wang, RSC Adv. 9 (2019) 33017–33022.
- T. Cai, H. Yang, K. Hills-Kimball, J.P. Song, H. Zhu, E. Hofman, W. Zheng, B.M. Rubenstein, O. Chen, J. Phys. Chem. Lett. 9 (2018) 7079-7084.

- [240] R.K. Behera, A. Dutta, D. Ghosh, S. Bera, S. Bhattacharyya, N. Pradhan, J. Phys. Chem. Lett. 10 (2019) 7916–7921.
- [241] W.B. Liu, B.Q. Yao, X.X. Li, A.A. Said, J.X. Lv, Z.L. Dong, W.J. Fan, X.W. Sun, Q.C. Zhang, ChemistrySelect 3 (2018) (1992) 11986–11991.
- [242] M. Zeng, F. Artizzu, J. Liu, S. Singh, F. Locardi, D. Mara, Z. Hens, R. Van Deun, ACS Appl. Nano Mater. 3 (2020) 4699–4707.
- [243] Y. Hu, F. Bai, X. Liu, Q. Ji, X. Miao, T. Qiu, S. Zhang, ACS Energy Lett. 2 (2017) 2219–2227.
- [244] Q.Q. Li, Y.F. Liu, P. Chen, J.S. Hou, Y. Sun, G.Y. Zhao, N. Zhang, J. Zou, J.Y. Xu, Y.Z. Fang, N. Dai, J. Phys. Chem. C 122 (2018) 29044–29050.
 [245] J.P. Ma, Y.M. Chen, L.M. Zhang, S.Q. Guo, J.D. Liu, H. Li, B.J. Ye, Z.Y. Li, Y. Zhou,
- [245] J.P. Ma, Y.M. Chen, L.M. Zhang, S.Q. Guo, J.D. Liu, H. Li, B.J. Ye, Z.Y. Li, Y. Zhou, B.B. Zhang, O.M. Bakr, J.Y. Zhang, H.T. Sun, J. Mater. Chem. C 7 (2019) 3037– 3048.
- [246] T.J. Milstein, K.T. Kluherz, D.M. Kroupa, C.S. Erickson, J.J. De Yoreo, D.R. Gamelin, Nano Lett. 19 (2019) 1931–1937.
- [247] H. Shao, X. Bai, H. Cui, G. Pan, P. Jing, S. Qu, J. Zhu, Y. Zhai, B. Dong, H. Song, Nanoscale 10 (2018) 1023–1029.
- [248] N. Chen, T. Cai, W. Li, K. Hills-Kimball, H. Yang, M. Que, Y. Nagaoka, Z. Liu, D. Yang, A. Dong, C.Y. Xu, R. Zia, O. Chen, ACS Appl. Mater. Interfaces 11 (2019) 16855–16863.
- [249] T. Cai, J. Wang, W. Li, K. Hills-Kimball, H. Yang, Y. Nagaoka, Y. Yuan, R. Zia, O. Chen, Adv. Sci. n/a (2020) 2001317.
- [250] S. Das, A. De, A. Samanta, J. Phys. Chem. Lett. 11 (2020) 1178–1188.